Journal of Cosmology and Astroparticle Physics
An IOP and SISSA journal

Gravitational waves from chiral phase transition in a conformally extended standard model

Mayumi Aoki[a] **and Jisuke Kubo**[b,c]

[a]Institute for Theoretical Physics, Kanazawa University, Kanazawa 920-1192, Japan
[b]Max-Planck-Institut für Physik (Werner-Heisenberg-Institut), Föhringer Ring 6, D-80805 München, Germany
[c]Department of Physics, University of Toyama, 3190 Gofuku, Toyama 930-8555, Japan

E-mail: mayumi@hep.s.kanazawa-u.ac.jp, jikubo4@gmail.com

Received October 18, 2019
Revised February 8, 2020
Accepted March 9, 2020
Published April 1, 2020

Abstract. The gravitational wave (GW) background produced at the cosmological chiral phase transition in a conformal extension of the standard model is studied. To obtain the bounce solution of coupled field equations we implement an iterative method. We find that the corresponding $O(3)$ symmetric Euclidean action S_3 divided by the temperature T has a simple behavior near the critical temperature T_C: $S_3/T \propto (1 - T/T_C)^{-\gamma}$, which is subsequently used to determine the transition's inverse duration β normalized to the Hubble parameter H. It turns out that $\beta/H \gtrsim 10^3$, implying that the sound wave period $\tau_{\rm sw}$ as an active GW source, too, can be much shorter than the Hubble time. We therefore compute $\tau_{\rm sw}H$ and use it as the reduction factor for the sound wave contribution. The signal-to-noise ratio (SNR) for Deci-Hertz Interferometer Gravitational Wave Observatory (DECIGO) and Big Bang Observer (BBO) is evaluated, with the result: $\mathrm{SNR}^{\rm DECIGO} \lesssim 1.2$ and $\mathrm{SNR}^{\rm BBO} \lesssim 12.0$ for five years observation, from which we conclude that the GW signal predicted by the model in the optimistic case could be detected at BBO.

Keywords: particle physics - cosmology connection, gravitational waves / theory

ArXiv ePrint: 1910.05025

https://doi.org/10.1088/1475-7516/2020/04/001

JCAP04(2020)001

Contents

1 Introduction

One of the central questions in particle physics today is: How to go beyond the standard model (SM), see, e.g., [1]. Indeed many theoretical suggestions have been made since ever [2]. The fact that the Higgs mass term is the only dimensionful parameter in the SM and the theory is perturbative — no Landau pole below the Planck scale [3–6] — may be regarded as a hint of how to go beyond the SM [1]. Even before the SM was proposed, John Wheeler [7] wished to remove all the dimensionful parameters from the fundamental equations. If we start with a theory, which at the classical level contains no dimensionful parameter such as mass parameter at all, an energy scale has to be generated by quantum effects. A quantum generation of the Higgs mass term from "nothing" would be along the line of John Wheeler's thought. There are two known mechanisms of "scalegenesis": One is the Coleman-Weinberg mechanism [8] that is based on improved perturbation theory and works thanks to scale anomaly [9, 10]. The other one is the dynamical scale symmetry breaking by strong dynamics in nonabelian gauge theories, e.g., Quantum Chromodynamics (QCD). We recall that about 99 % of the energy portion of the ordinary matter in the Universe — baryon — is generated by the nonperturbative effect in QCD [11], dynamical chiral symmetry breaking [12–14]. Several realistic models using the strong dynamics have been suggested in [15–20]: It has been found that not only the Higgs mass term, but also the dark matter mass [15–17, 19–22], contributing to 27 % of the total energy of the Universe [23], as well as the Planck mass [24] can be generated by dynamical scale symmetry breaking.

At finite temperature the real QCD does not undergo a phase transition (PT), rather a continuous change of crossover type [25]. However, for sufficiently small current quark

JCAP04(2020)001

masses, the system can undergo a first-order PT [26–29], and such a situation can be realized in hidden sector models [17, 30, 31] (see also [32] and references therein), in which dynamical breaking of scale symmetry takes place at energies higher than the SM scale. If the coupling of the hidden sector to the SM is very small, a chief signal from the hidden sector is the gravitational wave (GW) background produced at a first-order PT in a certain epoch of the Universe [33], see e.g. refs. [34, 35] for reviews.[1] This has been even more the case since the GWs have been detected on the earth [42–44].

In this paper we consider the model [21, 22], in which a robust energy scale, created by the chiral symmetry breaking in a strongly interacting QCD-like hidden sector, transmits via a SM singlet real scalar mediator S to the SM sector and generates the Higgs mass term to trigger electroweak (EW) symmetry breaking. We are particularly interested in the GW background produced at the cosmological chiral PT of the model.[2] The present work is an extension of ref. [31], where a few benchmark points in the parameter space have been chosen to study the GW background spectrum. We have decided to extend the analysis of ref. [31] from the following reasons:

a) The GW energy density depends strongly on the ratio of the duration time $\tau_{\rm PT} = 1/\beta$ of the first-order PT to the Hubble time $1/H$, i.e., $(\beta/H)^{-1}$ [33, 58–60]. Using effective field theories it has been shown [61] that, in contrast to the commonly assumed value of $\beta/H \sim O(10^2)$ [33, 62] (see also [34]), it is of order 10^4 in QCD like theories if the coupling to the SM is neglected, i.e., in the absence of the mediator S. This means a large suppression of the GW energy density. Here we will systematically look for a parameter space with smaller β/H, which leads to larger GW energy densities.

b) It turns out that the influence of the mediator S is an important factor to decrease β/H; the quartic self-coupling of S, λ_S, should be of order 10^{-3}, which is much smaller than the Higgs self-coupling $\lambda_H \sim O(10^{-1})$. Consequently, the mass of S denoted by m_S can become comparable with — or even smaller than — the Higgs mass m_h, and consequently the mixing of the Higgs h and S is no longer negligible, i.e., subject to the LHC constraint (see e.g. refs. [63, 64]). We will here take into account this LHC constraint.

c) To compute β/H one has to solve classical equations of motion and obtain the so-called bounce solution that describes a bubble appearing during a first-order PT [65]. In the model in question there are two fields that are involved in the problem, σ for the chiral condensate and S, so that we have to deal with a system of coupled differential equations. In ref. [31] we have employed a (modified) path-deformation method [66] to solve them. However, it has turned out that this method suffers from a large uncertainty and does not yield trustful results. Here we will employ another iterative method to realize a faster convergence of the iterative process.

d) The sound wave contribution to the GW spectrum will be the most dominant contribution in the model we will consider. A large β/H means a short duration of the first-order cosmological PT and hence a short sound wave period $\tau_{\rm sw}$ compared with $1/H$. However, the formula for the sound wave contribution to the GW spectrum has

[1] The crossover transition in the real QCD can influence the spectrum of the inflationary GW [36–41]. The frequency band of the damped GWs is what has been predicted by Witten [33].

[2] The GWs produced during a cosmological first-oder PT in classically scale invariant models have been recently studied in refs. [45–57].

JCAP04(2020)001

been derived from the numerical simulations for which a long-lasting source of the GW, i.e., $\tau_{\rm sw}H > 1$, is assumed [67]. If $\tau_{\rm sw}H < 1$, the sound wave is an active GW source only for a period shorter than the Hubble time. The above-mentioned formula therefore overestimates the sound wave contribution. Following refs. [68, 69] along with ref. [70], we calculate $\tau_{\rm sw}H$ and use it as the reduction factor for the sound wave contribution.

e) The signal-to-noise ratio (SNR) is an important measure to evaluate the detectability of the GW background of the model [71]. We will calculate the SNR for Deci-Hertz Interferometer Gravitational Wave Observatory (DECIGO) [72–74] and Big Bang Observer (BBO) [75–77].

In section 2 we outline the basic feature of the model; dynamical generation of the Higgs mass term, mass spectrum, the LHC constraint of the Higgs-S mixing, and dark matter (DM). Since the hidden sector of the model is strongly interacting, we use an effective theory for the dynamical chiral symmetry breaking — the Nambu-Jona-Lasinio (NJL) model [12–14] — as in refs. [17, 21, 22, 31], where our approximation method, the self-consistent mean-field approximation (SCMF) of refs. [78, 79], is also briefly elucidated in this section.

After a short review on the chiral PT in the hidden sector of the model we present, in section 3, our iterative method to obtain the bounce solution. We narrow the parameter space with smaller β/H. Two benchmark points are chosen for an orientation of the parameter space that we consider. In section 4 we discuss the GW spectrum. The above-mentioned reduction factor $\tau_{\rm sw}H$ for the sound wave contribution is computed in this section. We then calculate the SNR to evaluate the detectability of the GW signal at DECIGO and BBO. We also compare the GW spectrum for two chosen benchmark points with the power-law integrated sensitivity [71] of DECIGO and BBO. Section 5 is devoted to summary and conclusion.

2 The model

We consider a classically scale invariant extension of the SM studied in refs. [21, 22]. The model consists of a hidden $\mathrm{SU}(n_c)_H$ gauge sector coupled to the SM sector via a real singlet scalar S. The hidden sector Lagrangian $\mathcal{L}_{\rm H}$ of the total Lagrangian $\mathcal{L}_T = \mathcal{L}_{\rm H} + \mathcal{L}_{{\rm SM}+S}$ of the model is given as

$$\mathcal{L}_{\rm H} = -\frac{1}{2}\mathrm{Tr}\ F^2 + \mathrm{Tr}\ \bar{\psi}(i\gamma^\mu\partial_\mu + g_H\gamma^\mu G_\mu + g'Q\gamma^\mu B_\mu - \mathbf{y}S)\psi\,, \tag{2.1}$$

where G_μ is the gauge field for the hidden QCD, B_μ is the $\mathrm{U}(1)_Y$ gauge field,

$$B_\mu = \cos\theta_W A_\mu - \sin\theta_W Z_\mu\,, \quad g' = e/\cos\theta_W\,, \tag{2.2}$$

and the hidden vector-like fermions ψ_i $(i = 1, \ldots, n_f)$ belong to the fundamental representation of $\mathrm{SU}(n_c)_H$. The $\mathbf{y}$ is an $n_f \times n_f$ Yukawa coupling matrix which can be taken as a diagonal matrix without loss of generality, i.e. $\mathbf{y} = \mathrm{diag.}(y_1, \ldots, y_{n_f})$. Here the diagonal entries y_i are assumed to be positive. The $\mathcal{L}_{{\rm SM}+S}$ part contains the SM gauge and Yukawa interactions along with the scalar potential

$$V_{{\rm SM}+S} = \lambda_H(H^\dagger H)^2 + \frac{1}{4}\lambda_S S^4 - \frac{1}{2}\lambda_{HS}S^2(H^\dagger H)\,, \tag{2.3}$$

JCAP04(2020)001

where the portal coupling λ_{HS} is assumed to be positive, and $H^T = (H^+,\ (h + iG^0)\sqrt{2})$ is the SM Higgs doublet field with H^+ and G^0 as the would-be Nambu-Goldstone (NG) fields. The (tree-level) stability condition for the scalar potential is given by

$$\lambda_H > 0, \quad \lambda_S > 0, \quad 2\sqrt{\lambda_H \lambda_S} - \lambda_{HS} > 0\,. \tag{2.4}$$

Following refs. [17, 21, 22] we consider $n_f = n_c = 3$. In this case, the hidden chiral symmetry $\mathrm{SU}(3)_L \times \mathrm{SU}(3)_R$ is dynamically broken to its diagonal subgroup $\mathrm{SU}(3)_V$ by the nonzero chiral condensate $\langle\bar{\psi}\psi\rangle$, which implies the existence of 8 NG bosons. At the same time of the dynamical chiral symmetry breaking, the singlet scalar field S acquires a nonzero vacuum expectation value (VEV) due to the Yukawa interaction $-yS\bar{\psi}\psi$ in $\mathcal{L}_{\mathrm{H}}$, generating an explicit-chiral-symmetry-breaking mass term. Consequently, the NG bosons acquire their masses and can become DM candidates due to the remnant unbroken flavor group $\mathrm{SU}(3)_V$ (or its subgroup, depending on the choice of y_i) that can stabilise them. Finally, with the nonzero $v_S = \langle S\rangle$, the EW symmetry breaking is triggered by the Higgs mass term $+\frac{1}{2}\lambda_{HS} v_S^2 H^\dagger H$.

2.1 Nambu–Jona-Lasinio description

In order to analyze the strongly interacting hidden sector, we replace the Lagrangian $\mathcal{L}_{\mathrm{H}}$ (2.1) by the NJL Lagrangian that serves as an effective Lagrangian for the dynamical chiral symmetry breaking [12–14]:

$$\mathcal{L}_{\mathrm{NJL}} = \mathrm{Tr}\ \bar{\psi}(i\gamma^\mu\partial_\mu + g' Q\gamma^\mu B_\mu - \mathbf{y}S)\psi + 2G\ \mathrm{Tr}\ \Phi^\dagger\Phi + G_D\ (\det\Phi + \mathrm{h.c.})\,, \tag{2.5}$$

where

$$\Phi_{ij} = \bar{\psi}_i(1-\gamma_5)\psi_j = \frac{1}{2}\sum_{a=0}^{8}\lambda^a_{ji}\,[\,\bar{\psi}\lambda^a(1-\gamma_5)\psi\,]\,, \tag{2.6}$$

and $\lambda^a (a = 1,\ldots,8)$ are the Gell-Mann matrices with $\lambda^0 = \sqrt{2/3}\ \mathbf{1}$. The dimensionful parameters G and G_D have canonical dimensions of -2 and -5, respectively. In order to deal with the nonrenormalizable Lagrangian (2.5) we work in the SCMF approximation of refs. [78, 79]. The mean fields σ_i $(i = 1,2,3)$ and ϕ_a $(a = 0,\ldots,8)$ are defined in the "Bardeen-Cooper-Schrieffer" vacuum as

$$\sigma_i = -4G\,\langle\bar{\psi}_i\psi_i\rangle\ , \quad \phi_a = -2iG\,\langle\bar{\psi}_i\gamma_5\lambda^a\psi_i\rangle\ , \tag{2.7}$$

where the CP-even mean fields corresponding to the non-diagonal elements of $\langle\bar{\psi}_i\psi_j\rangle$ are suppressed, because they do not play any role for our purpose. Splitting the NJL Lagrangian $\mathcal{L}_{\mathrm{NJL}}$ into two parts as $\mathcal{L}_{\mathrm{NJL}} = \mathcal{L}_{\mathrm{MFA}} + \mathcal{L}_I$ where $\mathcal{L}_I$ is normal ordered (i.e., $\langle 0|\mathcal{L}_I|0\rangle = 0$), we find the Lagrangian in the SCMF approximation $\mathcal{L}_{\mathrm{MFA}}$ in the $\mathrm{SU}(3)_V$ limit as[3]

$$\begin{aligned}\mathcal{L}_{\mathrm{MFA}} = {}& \mathrm{Tr}\ \bar{\psi}(i\partial\!\!\!/ - M + g' Q\gamma^\mu B_\mu)\psi - i\,\mathrm{Tr}\ \bar{\psi}\gamma_5\phi\psi - \frac{1}{8G}\left(3\sigma^2 + 2\sum_{a=1}^{8}\phi_a\phi_a\right)\\ &+ \frac{G_D}{8G^2}\left(-\mathrm{Tr}\ \bar{\psi}\phi^2\psi + \sum_{a=1}^{8}\phi_a\phi_a\,\mathrm{Tr}\ \bar{\psi}\psi + i\sigma\,\mathrm{Tr}\ \bar{\psi}\gamma_5\phi\psi + \frac{\sigma^3}{2G} + \frac{\sigma}{2G}\sum_{a=1}^{8}(\phi_a)^2\right)\end{aligned} \tag{2.8}$$

[3]The mean-field Lagrangian $\mathcal{L}_{\mathrm{MFA}}$ in the case of broken $\mathrm{SU}(3)_V$ can be found in ref. [22].

JCAP04(2020)001

with $\phi = \sum_{a=1}^{8} \phi_a \lambda^a$ and $\sigma = \sigma_1 = \sigma_2 = \sigma_3$. Here ϕ_0 has been suppressed and the constituent fermion mass M is given by

$$M(S,\sigma) = \sigma + yS - \frac{G_D}{8G^2}\sigma^2 \,, \text{where } y = y_1 = y_2 = y_3 \,. \tag{2.9}$$

The one-loop effective potential obtained from $\mathcal{L}_{\rm MFA}$ (2.8) can be obtained by integrating out the hidden fermions:

$$V_{\rm NJL}(S,\sigma) = \frac{3}{8G}\sigma^2 - \frac{G_D}{16G^3}\sigma^3 - 3n_c I_0(M,\Lambda_H) \,. \tag{2.10}$$

Here the function I_0 is given by

$$I_0(M,\Lambda) = \frac{1}{16\pi^2}\left[\Lambda^4 \ln\left(1+\frac{M^2}{\Lambda^2}\right) - M^4 \ln\left(1+\frac{\Lambda^2}{M^2}\right) + \Lambda^2 M^2\right] \tag{2.11}$$

with a four-dimensional momentum cutoff Λ, where we denote the cutoff in the hidden sector by Λ_H. For a certain interval of the dimensionless parameters $G^{1/2}\Lambda_H$ and $(-G_D)^{1/5}\Lambda_H$ we have $\langle\sigma\rangle \neq 0$ and $\langle S\rangle \neq 0$ [17, 21, 22]. It is then meant that the dynamics of the hidden sector creates a nonvanishing chiral condensate $\langle 0|\bar{\psi}_i\psi_i|0\rangle \neq 0$. One can see that the potential $V_{\rm NJL}(S,\sigma)$ is asymmetric in σ owing to the last term in the NJL Lagrangian (2.5) and also from the constituent mass M (2.9), which is the reason that the chiral PT at finite temperature can become of first order. It is noted that the mean fields σ and ϕ_a are non-propagating classical fields at the tree level. Therefore, their kinetic terms are generated by integrating out the hidden fermions at the one-loop level, which will be seen in section 2.2 where two point functions are calculated.

The NJL parameters for the hidden QCD sector are obtained by scaling-up the values of G, G_D and the cutoff Λ from QCD hadron physics. Following refs. [17, 21, 22] we assume that the dimensionless combinations

$$G^{1/2}\Lambda_H = 1.82 \,, \qquad (-G_D)^{1/5}\Lambda_H = 2.29 \,, \tag{2.12}$$

which are satisfied for the real-world hadrons, remain unchanged for a higher scale of Λ_H. Therefore, the free parameters of the (effective) model are: $\lambda_H, \lambda_S, \lambda_{HS}$ and Λ_H. Once these parameters are fixed, the VEVs of $\sigma\,, S$ and h can be obtained through the minimization of the scalar potential $V_{\rm SM+S} + V_{\rm NJL}$ where we choose these parameters so as to satisfy $m_h = 125\,\text{GeV}$ and $\langle h\rangle = 246$ GeV.

2.2 Mass spectrum

Once the VEVs of σ, S and h are obtained, the scalar mass spectrum can be calculated from the corresponding two point functions at one-loop in which the hidden fermions are circulating. The CP even scalars h, S and σ mix with each other. The two point functions at the one-loop level $\Gamma_{AB}(A, B = h, S, \sigma)$ in the $\mathrm{SU}(3)_V$ flavor symmetry limit are given by

$$\Gamma_{hh}(p^2) = p^2 - 3\lambda_H \langle h\rangle^2 + \frac{1}{2}\lambda_{HS}\langle S\rangle^2 \,, \quad \Gamma_{hS} = \lambda_{HS}\langle h\rangle\langle S\rangle \,, \quad \Gamma_{h\sigma} = 0 \,,$$

$$\Gamma_{SS}(p^2) = p^2 - 3\lambda_S \langle S\rangle^2 + \frac{1}{2}\lambda_{HS}\langle h\rangle^2 - y^2 3n_c I_{\varphi^2}(p^2, M, \Lambda_{\rm H}) \,, \tag{2.13}$$

$$\Gamma_{S\sigma}(p^2) = -y\left(1 - \frac{G_D\langle\sigma\rangle}{4G^2}\right) 3n_c I_{\varphi^2}(p^2, M, \Lambda_{\rm H}) \,, \tag{2.14}$$

$$\Gamma_{\sigma\sigma}(p^2) = -\frac{3}{4G} + \frac{3G_D\langle\sigma\rangle}{8G^3} - \left(1 - \frac{G_D\langle\sigma\rangle}{4G^2}\right)^2 3n_c I_{\varphi^2}(p^2, M, \Lambda_{\rm H}) + \frac{G_D}{G^2} 3n_c I_V(M, \Lambda_{\rm H}) \,.$$

JCAP04(2020)001

Here the loop functions are defined as

$$I_{\varphi^2}(p^2, M, \Lambda) = \int_\Lambda \frac{d^4k}{i(2\pi)^4} \frac{\mathrm{Tr}(\not{k} + \not{p} + M)(\not{k} + M)}{((k+p)^2 - M^2)(k^2 - M^2)}\,, \tag{2.15}$$

$$I_V(M, \Lambda) = \int_\Lambda \frac{d^4k}{i(2\pi)^4} \frac{M}{(k^2 - M^2)} = -\frac{1}{16\pi^2} M \left[\Lambda^2 - M^2 \ln\left(1 + \frac{\Lambda^2}{M^2}\right)\right]. \tag{2.16}$$

The flavor eigenstates (h, S, σ) and the mass eigenstates h_i $(i = 1, 2, 3)$ are related by

$$\begin{pmatrix} h \\ S \\ \sigma \end{pmatrix} = \begin{pmatrix} \xi_h^{(1)} & \xi_h^{(2)} & \xi_h^{(3)} \\ \xi_S^{(1)} & \xi_S^{(2)} & \xi_S^{(3)} \\ \xi_\sigma^{(1)} & \xi_\sigma^{(2)} & \xi_\sigma^{(3)} \end{pmatrix} \begin{pmatrix} h_1 \\ h_2 \\ h_3 \end{pmatrix}. \tag{2.17}$$

The squared masses $m_{h_i}^2$ are determined by the zeros of the two point functions at the one-loop level, i.e. $\Gamma_{AB}(m_{h_i}^2)\xi_B^{(i)} = 0$.

In this model the DM candidates are the NG bosons in the hidden sector which are CP-odd scalars ϕ_a in eq. (2.7), i.e. the dark mesons. The two point function at the one-loop level for the DM candidate is (in the $\mathrm{SU}(3)_V$ flavor symmetry limit)

$$\Gamma_{\mathrm{DM}}(p^2) = -\frac{1}{2G} + \frac{G_D\langle\sigma\rangle}{8G^3} + \left(1 - \frac{G_D\langle\sigma\rangle}{8G^2}\right)^2 2n_c I_{\phi^2}(p^2, M, \Lambda_{\mathrm{H}}) + \frac{G_D}{G^2} n_c I_V(M, \Lambda_{\mathrm{H}})\,, \tag{2.18}$$

where the loop function $I_{\phi^2}(p^2, M, \Lambda)$ is given by

$$I_{\phi^2}(p^2, M, \Lambda) = \int_\Lambda \frac{d^4k}{i(2\pi)^4} \frac{\mathrm{Tr}(\not{k} - \not{p} + M)\gamma_5(\not{k} + M)\gamma_5}{((k-p)^2 - M^2)(k^2 - M^2)}\,. \tag{2.19}$$

The mass of the DM is obtained from $\Gamma_{\mathrm{DM}}(m_{\mathrm{DM}}^2) = 0$.

2.3 LHC constraint on λ_{HS}

The size of the portal coupling λ_{HS} controls the $h - S$ mixing. Since in the parameter space we will consider the Yukawa coupling y is small, i.e. of order 10^{-3} (see eq. (4.12)), the mixing $\Gamma_{S\sigma}$ (2.14) is also small, so that we will neglect it in the following discussions. (We will also neglect the last term of Γ_{SS} (2.13), because it is proportional to y^2.) Therefore, the $h - S$ mixing can be written as

$$\begin{pmatrix} h_1 \\ h_2 \end{pmatrix} = \begin{pmatrix} \cos\theta & \sin\theta \\ -\sin\theta & \cos\theta \end{pmatrix} \begin{pmatrix} h \\ S \end{pmatrix} \tag{2.20}$$

with $(\cos\theta\,, -\sin\theta\,, 0) \simeq (\xi_h^{(1)}\,, \xi_h^{(2)}\,, \xi_h^{(3)})$ which is defined in eq. (2.17). Here we identify h_1 with the SM Higgs having mass $m_h \simeq 0.125\,\mathrm{TeV}$, i.e., $m_h = m_{h_1}$ and $m_S = m_{h_2}$. The $h - S$ mixing is constrained by LHC data (see e.g. refs. [63, 64] and references thererin). In the left panel of figure 1 we plot $|\sin\theta|$ versus m_S and in the right panel m_S (purple) and m_{DM} (green) versus λ_{HS} both at $\lambda_S = 0.001$. We vary λ_{HS} between 0.0001 and 0.018 and y between 0.001 and 0.00172. (Why we consider y in this interval will be explained in section 3.) As we see from the left panel, there are two branches; $m_S < m_h$ and $m_S > m_h$, and on each branch there exist a (blue) region, I and II, that is allowed by LHC. The band of m_{DM}

JCAP04(2020)001

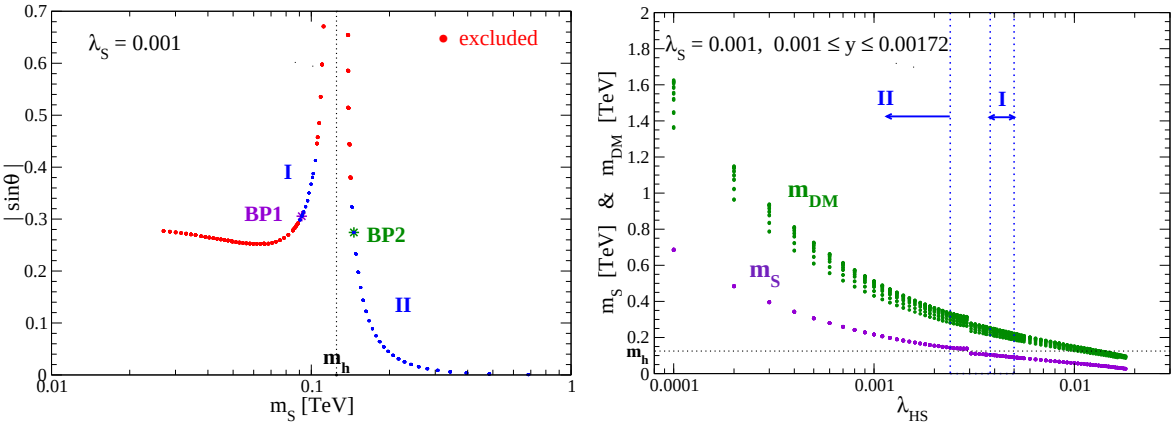

Figure 1. Left: $|\sin\theta|$ vesus m_S at $\lambda_S = 0.001$, where we vary λ_{HS} between 0.0001 and 0.018 and y between 0.001 and 0.00172. There are two branches; $m_S < m_h$ and $m_S > m_h$, and on each branch there exist a (blue) region (I and II) that is allowed by LHC. Two benchmark points we consider are marked by BP1 (purple) and BP2 (green). Right: m_S (purple) and $m_{\rm DM}$ (green) vesus λ_{HS} at $\lambda_S = 0.001$.

in the right panel can be seen, because it sensitively depends on y, while m_S is insensitive against y. From each allowed region we choose a representative point, BP1 and BP2, to get an orientation in the parameter space, especially when discussing the GW spectrum later on:

$$\begin{aligned}
&\text{BP1}: \lambda_S = 0.001\,,\ \lambda_{HS} = 0.00485\,,\ y = 0.00172\,,\ \lambda_H = 0.1238\,,\ \Lambda_H = 4.322\,\text{TeV}\,,\\
&\text{BP2}: \lambda_S = 0.001\,,\ \lambda_{HS} = 0.00230\,,\ y = 0.00170\,,\ \lambda_H = 0.1325\,,\ \Lambda_H = 6.606\,\text{TeV}\,.
\end{aligned} \tag{2.21}$$

2.4 Dark matter

Due to the vector-like flavor symmetry (i.e. $\mathrm{SU}(3)_V$ or its subgroup), the dark mesons are good DM candidates. As we see from figure 1, the mass of the real singlet m_S is smaller than the DM mass $m_{\rm DM}$, so that the DM can annihilate into two Ss in principle. However, this annihilation cross section is negligibly small because it is $\propto y^4 \lesssim 10^{-11}$ in the parameter space of interest. To explain the observed value for the relic DM abundance in this circumstance, we assume a hierarchy in the Yukawa couplings: $y_1 = y_2 < y_3$ (which breaks $\mathrm{SU}(3)_V$ down to $\mathrm{SU}(2)_V \times \mathrm{U}(1)$ explicitly), where y_3 should not differ very much from y_2 [22]. Under this assumption, the dark mesons fall into three categories, $\tilde{\pi} = \left\{\tilde{\pi}^\pm,\ \tilde{\pi}^0\right\}, \tilde{K} = \left\{\tilde{K}^\pm,\ \tilde{K}^0,\ \bar{\tilde{K}}^0\right\}$ and $\tilde{\eta}$. Here the dark mesons are given like the real-world mesons:

$$\begin{aligned}
&\tilde{\pi}^\pm \equiv (\phi_1 \mp i\phi_2)/\sqrt{2}\,, \qquad \tilde{\pi}^0 \equiv \phi_3\,,\\
&\tilde{K}^\pm \equiv (\phi_4 \mp i\phi_5)/\sqrt{2}\,,\ \ \tilde{K}^0(\bar{\tilde{K}}^0) \equiv (\phi_6 + (-)i\phi_7)/\sqrt{2}\,,\ \ \tilde{\eta}^8 \equiv \phi_8\,,
\end{aligned} \tag{2.22}$$

where $\tilde{\eta}^8$ will mix with $\tilde{\eta}^0$ to form the mass eigenstates $\tilde{\eta}$ and $\tilde{\eta}'$. The states in the same category have the same mass, $m_{\tilde{\pi}^0} = m_{\tilde{\pi}^\pm}(\equiv m_{\tilde{\pi}})$ and $m_{\tilde{K}^\pm} = m_{\tilde{K}^0} = m_{\bar{\tilde{K}}^0}(\equiv m_{\tilde{K}})$, with $m_{\tilde{\pi}} < m_{\tilde{K}} < m_{\tilde{\eta}}$, where the differences among $m_{\tilde{\pi}}$, $m_{\tilde{K}}$ and $m_{\tilde{\eta}}$ are small because of the small difference between $y_1 = y_2$ and y_3. The heavier state $\tilde{\eta}$ is an unstable NG boson which can mainly decay into two γs. On the other hand, the $\tilde{\pi}$ and $\tilde{K}$ are stable due to the $\mathrm{SU}(2)_V$ flavor symmetry and become the DM. Since the mass difference among $\tilde{\pi}, \tilde{K}$ and $\tilde{\eta}$ are small, the DM annihilation into a pair of heavier DMs and/or $\tilde{\eta}$s, which are kinematically forbidden at zero temperature, can become operative. In ref. [22] it has been shown that the

JCAP04(2020)001

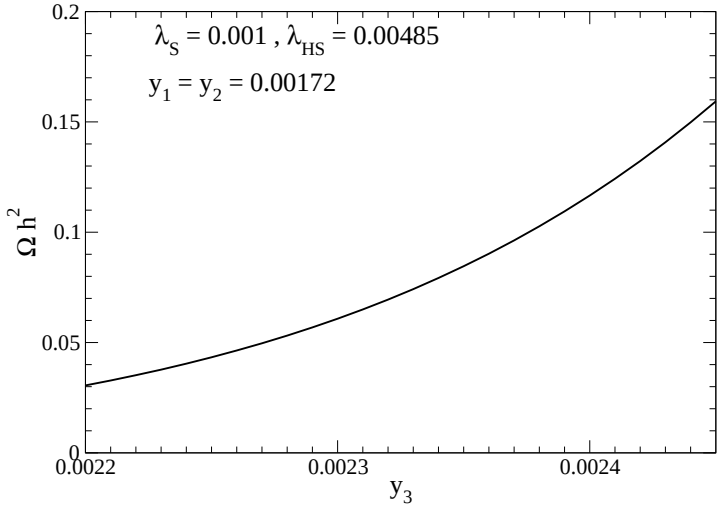

Figure 2. The total DM relic abundance Ωh^2 with the $\mathrm{U}(1)_Y$ hypercharge $Q = 1/3$ vesus y_3, where we have fixed other parameters at the benchmark point BP1 defined in eq. (2.21).

inverse conversion $\tilde{\pi}\tilde{\pi}, \tilde{K}\tilde{K} \to \tilde{\eta}\tilde{\eta} \to \gamma\gamma\gamma\gamma$ can play a significant role to make the DM relic abundance realistic. This mechanism works only if the $\mathrm{SU}(3)_V$ falvor symmetry is broken into its subgroup.[4]

In figure 2 we show the total DM relic abundance $\Omega h^2 = \Omega_\pi h^2 + \Omega_K h^2$ with the $\mathrm{U}(1)_Y$ hypercharge $Q = 1/3$ as a function of y_3, where the other parameters are chosen for the benchmark point BP1 defined in eq. (2.21), and h is the dimensionless Hubble parameter. We see from this figure that the DM relic abundance at $y_3 \simeq 0.0024$ can coincide with the experimentally observed value [23].[5]

3 Chiral phase transition and bounce solution

3.1 Effective potential and chiral phase transition

The EW and chiral PTs in our model (2.1) have been studied in refs. [17, 31] in some detail. For a phenomenologically viable region of the parameter space, the EW PT occurs — with decreasing temperature — after the chiral PT takes place in a hidden sector. Therefore, the VEV of h vanishes during the chiral PT, so that we set $\langle h \rangle = 0$ in investigating the chiral PT. Accordingly, we analyze the following scalar potential at finite temperature:

$$V_{\mathrm{EFF}}(S, \sigma, T) = V^{h\to 0}_{\mathrm{SM}+S}(S) + V_{\mathrm{NJL}}(S, \sigma) + V_{\mathrm{CW}}(S) + V_{\mathrm{FTB}}(S, T) + V_{\mathrm{FTF}}(S, \sigma, T)\,, \tag{3.1}$$

where $V_{\mathrm{SM}+S}$ and $V_{\mathrm{NJL}}(S, \sigma)$ are given in eqs. (2.3) and (2.10), respectively,

$$V_{\mathrm{CW}}(S) = \frac{m_S^4(S)}{64\pi^2}\left[\ln(S^2/\langle S\rangle^2) - 1/2\right]\,, \tag{3.2}$$

$$V_{\mathrm{FTB}}(S, T) = \frac{T^4}{2\pi^2}\left[J_B(M_S(S)/T) - J_B(|\lambda_S/4 - \lambda_{HS}/6|^{1/2})\right]\,, \tag{3.3}$$

[4] In the model considered in ref. [31] the flavor group $\mathrm{SU}(3)_V$ is unbroken and the hidden fermions have no coupling with the $\mathrm{U}(1)_Y$ gauge boson.

[5] Though the portal coupling λ_{HS} is very small $\sim 10^{-3}$, the singlet scalar S decays via the $h - S$ mixing into the SM particles much before Big Bang Nucleosynthesis (BBN): $\Gamma(S \to \text{SM particles})/H \simeq \sin^2\theta\,\Gamma(h \to \text{SM particles})/H \sim \sin^2\theta \times 10^{22}$ at $T = 1\,\mathrm{MeV}$.

JCAP04(2020)001

$$V_{\rm FTF}(S,\sigma,T) = -6n_c\frac{T^4}{\pi^2}\left[J_F(M(S,\sigma)/T) - J_F(0)\right]\,, \tag{3.4}$$

$$M_S^2 = m_S^2(S) + \left(\frac{\lambda_S}{4} - \frac{\lambda_{HS}}{6}\right)T^2 \text{ with } m_S^2(S) = 3\lambda_S S^2\,, \tag{3.5}$$

and $M(S,\sigma)$ is given in (2.9). The thermal functions are

$$\begin{aligned} J_{F/B}(u) &= \int_0^\infty dx x^2 \ln\left(1 \pm e^{-\sqrt{x^2+u^2}}\right) \\ &= \sum_{j=1}^{\infty}(\mp 1)^{(1+j)}(u^2/j^2)K_2(j\,u)\,, \end{aligned} \tag{3.6}$$

where $K_2(j\,u)$ is the modified Bessel function of the second kind of order two, and we will truncate the sum at $j = 10$.[6] In $V_{\rm FTB}(S,T)$ and $V_{\rm FTF}(S,\sigma,T)$ we have subtracted the (temperature-dependent) constant terms such that $V_{\rm FTB}(0,T) = V_{\rm FTF}(0,0,T) = 0$. We first note that the role of the singlet scalar S becomes more important for smaller λ_S. To see this, we will consider $V_{\rm NJL}(S,\sigma)$ for small y:

$$V_{\rm NJL}(S,\sigma) = V_{\rm NJL}(0,\sigma) - \frac{3n_c\Lambda_H^2\sigma}{4\pi^2}yS + O((yS)^2)\,. \tag{3.7}$$

Since, neglecting the portal coupling λ_{HS}, the scalar potential $V_{\rm SM+S}$ becomes $\lambda_H(H^\dagger H)^2 + (1/4)\lambda_S S^4$, we find

$$v_S^3 = \langle S\rangle^3 \simeq \frac{3n_c\Lambda_H^2 v_\sigma}{4\pi^2}\left(\frac{y}{\lambda_S}\right)\,. \tag{3.8}$$

Therefore, the deviation from the pure NJL model (i.e. without the singlet scalar S) is larger for smaller λ_S and larger y. The above feature remains at finite temperature, as we can see from figure 3, where we show v_S/v_σ against λ_S at the critical temperature T_C for $y = 0.001\,, \lambda_{HS} = 0$.[7] In figure 4 we plot v_σ/T (blue) and v_S/T (red) as a function of T/Λ_H for $\lambda_S = 0.005, \lambda_{HS} = 0$ and $y = 0.001$ (upper left panel) and 0.007 (upper right panel), respectively. We see that the chiral PT is no longer a strong first-order PT at $y = 0.007$. The lower panels show the case for $\lambda_S = 0.001, \lambda_{HS} = 0$ and $y = 0.00172$ (left) and 0.0045 (right).

3.2 Bounce solution

One of the main quantities in discussing the stochastic GW background produced by a first-order PT in the expanding Universe is the duration time of the first-order PT, $\tau_{\rm pt} = \beta^{-1}$, which should be compared with the inverse rate of the expansion H^{-1} [33, 58–60]. In fact

[6] The error of the approximate function $J_{F(B)}(u; j_{\rm max})$ with the truncation at $j = j_{\rm max}$ is $\Delta J_{F(B)} = \left|\, J_{F(B)}(u) - J_{F(B)}(u; j_{\rm max})\,\right|$. For $j_{\rm max} = 10$, $\Delta J_F < 5\times 10^{-5}$ and $\Delta J_B < 3\times 10^{-4}$ are satisfied. So, with $j_{\rm max} = 10$, the error in $\Delta(V_{\rm EFF}/T^4)$ is less than 10^{-4}. Since we are interested in the behavior of $V_{\rm EFF}$ near the critical temperature T_C, we obtain $\Delta(V_{\rm EFF}/\Lambda_H^4) < 10^{-8}$ because $T_C/\Lambda_H \sim 0.1$. This accuracy is sufficient for our purpose.

[7] The absolute scale of the hidden sector (i.e. Λ_H) can be anything when the hidden sector has no coupling with the SM sector. This happens, for instance, when λ_{HS} is set equal to zero. Nevertheless, dimensionless quantities have their meaning. As we see from eqs. (2.3) and (3.1) the λ_{HS} dependence of the effective potential is very small if $\langle h\rangle = 0$: It enters only in the thermal mass of S as one can see in eq. (3.5).

JCAP04(2020)001

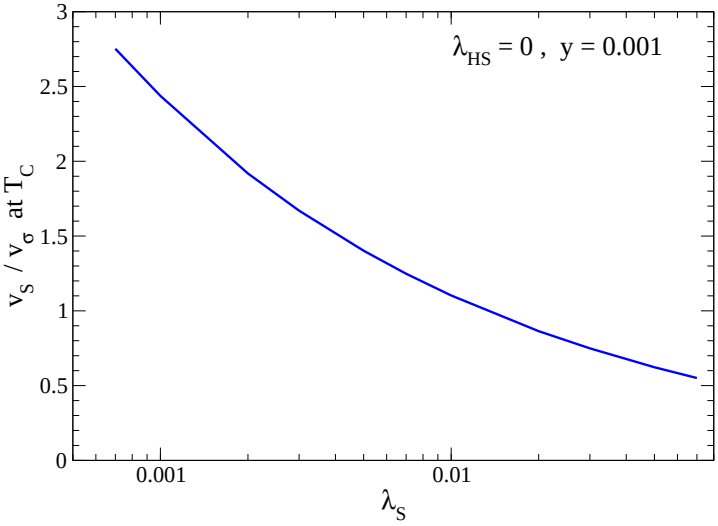

Figure 3. v_S/v_σ at the critical temperature T_C against λ_S. We see that the smaller λ_S is, the larger the ratio v_S/v_σ becomes, which means more deviation from the pure NJL (i.e. without the singlet scalar S).

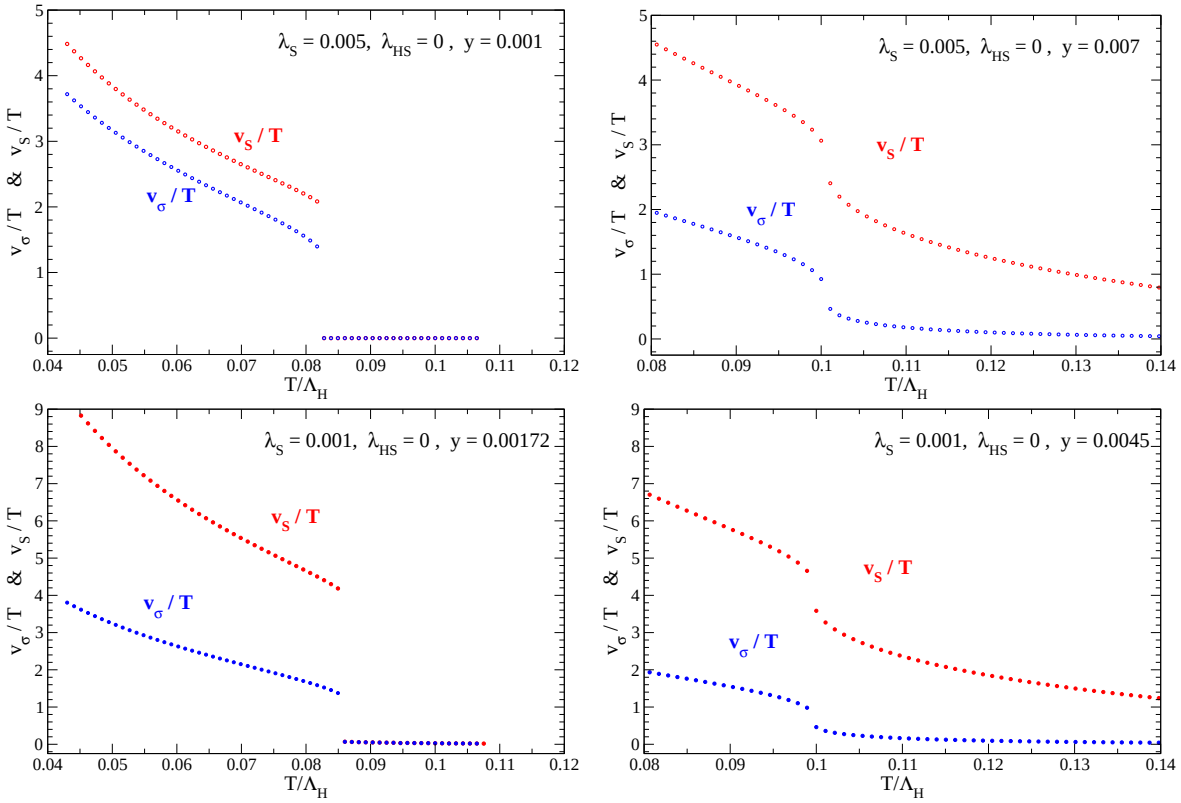

Figure 4. Upper (lower) left: v_σ/T (blue) and v_S/T (red) against T/Λ_H for $\lambda_S = 0.005$ (0.001), $\lambda_{HS} = 0, y = 0.001$ (0.00172), showing a strong first-order PT. Upper (lower) right: The same with $y = 0.007$ (0.0045), showing a transition of cross-over type.

JCAP04(2020)001

the GW energy density increases — depending on the nature of its source — linearly or even quadratically with $(\beta/H)^{-1}$ (see eqs. (4.21), (4.24) and (4.27)), while its peak frequency increases linearly with β/H (see eqs. (4.23), (4.26) and (4.29)). In ref. [61] it has been found that β/H is of order 10^4 in the pure NJL model, so that $\Omega_{\rm GW}$, the spectral GW energy density normalized to the critical energy density, is considerably suppressed. Therefore, we consider here a parameter space in which the deviation from the pure NJL model is large. From the discussion of section 3.1 we can infer that the area with small λ_S and large y is an optimistic parameter space, where y should not be too large for a strong first-order chiral PT to be realized. It turns out that $\lambda_S \sim O(10^{-3})$ is an optimistic magnitude for λ_S, and in the following discussions we concentrate on the parameter space with $\lambda_S = 0.001$.

To obtain β/H we have to compute the value of the corresponding $O(3)$ symmetric Euclidean action S_3 [65]. The mean field σ, introduced as an auxiliary field at the tree level in the mean-field approximation, is a driving force for the chiral PT. As it has been discussed in section 2.2 the mean field σ can be promoted to a propagating quantum field at one loop, which also applies at finite temperature. The kinetic term for σ at finite temperature has been correctly computed in ref. [61]. Quoting the result of ref. [61], the $O(3)$ symmetric action S_3 can be written as

$$S_3(T) = 4\pi \int dr r^2 \left[\frac{Z_\sigma^{-1}(S,\sigma,T)}{2} \left(\frac{d\sigma}{dr}\right)^2 + \frac{1}{2}\left(\frac{dS}{dr}\right)^2 + V_{\rm EFF}(S,\sigma,T) \right], \tag{3.9}$$

where r is the radial coordinate of the 3-dimensional space, and $V_{\rm EFF}(S,\sigma,T)$ is given in eq. (3.1). $Z_\sigma(S,\sigma,T)$ is the wave function renormalization "constant" at finite temperature [61]:

$$\begin{aligned}
Z_\sigma^{-1}(\sigma,S,T) &= \frac{n_c n_f}{2\pi^2}\left[1 - \frac{G_D}{4G^2}\sigma\right]^2 \\
\times \Bigg\{ &-\frac{\Lambda_H^2}{4(\Lambda_H^2+M^2)} + \frac{1}{4}\ln(1+\Lambda_H^2/M^2) + \frac{\Lambda_H^4}{8(\Lambda_H^2+M^2)^2} - \frac{\Lambda_H^4(\Lambda_H^2+3M^2)}{6(\Lambda_H^2+M^2)^3} \\
&+ \int_0^\infty dx x^2 \Bigg[-\frac{1+e^{\omega/T}(1+\omega/T)}{(1+e^{\omega/T})^2(\omega/T)^3} - (M/T)^2 \frac{3+e^{\omega/T}(6+3\omega/T-(\omega/T)^2)}{4(1+e^{\omega/T})^3(\omega/T)^5} \\
&-(M/T)^2 \frac{e^{2\omega/T}(3+3\omega/T+(\omega/T)^2)}{4(1+e^{\omega/T})^3(\omega/T)^5} \\
&+(M/T)^4 \frac{15+e^{\omega/T}(45+15\omega/T-6(\omega/T)^2+(\omega/T)^3)+e^{2\omega/T}(45+30\omega/T-4(\omega/T)^2)}{6(1+e^{\omega/T})^4(\omega/T)^7} \\
&+(M/T)^4 \frac{e^{3\omega/T}(15+15\omega/T+6(\omega/T)^2)+(\omega/T)^3)}{6(1+e^{\omega/T})^4(\omega/T)^7} \Bigg] \Bigg\},
\end{aligned} \tag{3.10}$$

where

$$\omega/T = [x^2 + (M/T)^2]^{1/2}, \tag{3.11}$$

and M is given in eq. (2.9).

The equations of motion for the action (3.9) read

$$\frac{d^2\sigma}{dr^2} + \frac{2}{r}\frac{d\sigma}{dr} + \frac{1}{2}\frac{\partial \ln Z_\sigma^{-1}(S,\sigma,T)}{\partial\sigma}\left(\frac{d\sigma}{dr}\right)^2 = Z_\sigma(S,\sigma,T)\frac{\partial V_{\rm EFF}(S,\sigma,T)}{\partial\sigma}, \tag{3.12}$$

$$\frac{d^2S}{dr^2} + \frac{2}{r}\frac{dS}{dr} - \frac{1}{2}\frac{\partial Z_\sigma^{-1}(S,\sigma,T)}{\partial S}\left(\frac{d\sigma}{dr}\right)^2 = \frac{\partial V_{\rm EFF}(S,\sigma,T)}{\partial S}, \tag{3.13}$$

JCAP04(2020)001

and the boundary conditions for the bounce solution are given by [65]

$$\left.\frac{d\sigma}{dr}\right|_{r=0} = 0\,, \quad \left.\frac{dS}{dr}\right|_{r=0} = 0\,, \quad \lim_{r\to\infty}\sigma(r) = 0\,, \quad \lim_{r\to\infty} S(r) = 0\,. \tag{3.14}$$

The bounce solution describes a bubble, where $r = 0$ is the center of the bubble, inside of which the chiral symmetry is broken. The bubble however has no sharp boundary, but $\sigma(r)$ and $S(r)$ at $r \simeq r_w$ drop sharply from a finite value to a small value (see figure 5) so that r_w can be understood as the position of the bubble wall: We may say in a less precise way that inside of the wall the chiral symmetry is broken and in the outside of the wall it is unbroken. In the one-dimensional case, in which there exists only one scalar degree of freedom as an order parameter, we can obtain a bounce solution by using the so-called overshooting/undershooting method [80]. However, this is an extremely cumbersome method in a multi-dimensional case, because a set of certain initial conditions have to be simultaneously fine tuned. An appropriate method is the path deformation method [66]. But to minimize the problem associated with the complicated structure of the wave function renormalization (3.10), we here use another iterative method, which we will describe below.

One round of the calculation consists of two steps. At the first step in the $n^{\rm th}$ round, we solve the differential equation (3.12) for $\sigma(r)$ with $S(r) = S_{(n-1)}(r)$, where $S_{(n-1)}(r)$ is obtained in the $(n-1)^{\rm th}$ round. The solution is denoted by $\sigma_{(n)}(r)$. At the second step in the $n^{\rm th}$ round, we solve the differential equation (3.13) for $S(r)$ with $\sigma(r) = \sigma_{(n)}(r)$ to obtain $S_{(n)}(r)$. Then, using $\sigma_{(n)}(r)$ and $S_{(n)}(r)$ we compute S_3/T in the $n^{\rm th}$ round and denote it by $(S_3/T)_{(n)}$. Since each step is a one-dimensional problem, we apply the overshooting/undershooting method. Of course, there is no mathematical warranty that the iterative process converges: It depends strongly on $S_{(0)}$ that is needed to carry out the first step in the first round, i.e., to obtain $\sigma_{(1)}(r)$. Here we assume that $S_{(0)}$ is a function of σ and choose it as a straight line linking the origin of the field space ($\sigma = S = 0$) and the position (v_σ, v_S) of the minimum of $V_{\rm EFF}(S, \sigma, T < T_C)$:

$$S_{(0)}(\sigma) = \frac{v_S}{v_\sigma}\sigma\,. \tag{3.15}$$

In the upper (lower) left panel of figure 5, we show $\sigma_{(n)}(r)$ and $S_{(n)}(r)$ with $n = 1$ (blue), 2 (red), 3 (black) for $\lambda_S = 0.003\ (0.001)$, $\lambda_{HS} = 0$, $y = 0.001\,(0.00172)$, $T_C/\Lambda_H = 0.0796\,(0.0843)$, $T/\Lambda_H = 0.0769\,(0.0798)$. We find also

$$\begin{aligned} (S_3/T)_{(1)} &= 144.4\,(153.5)\,, \quad (S_3/T)_{(2)} = 140.9\,(140.0)\,, \\ (S_3/T)_{(3)} &= 141.5\,(144.7)\,, \quad (S_3/T)_{(4)} = 140.8\,(142.2)\,. \end{aligned} \tag{3.16}$$

So, the convergence of the iterative process, described above, is quite fast. We have calculated S_3/T for several values of $x = T/T_C$ in the second round and found that S_3/T for $x < 1$ can be nicely fitted with a simple function [61, 62]

$$\frac{S_3}{T}(x) = b\,(1-x)^{-\gamma}\,. \tag{3.17}$$

This is shown in the upper (lower) right panel of figure 5 for λ_S=0.003 (0.001), λ_{HS} =0, y=0.001 (0.00172). The blue dotted line is the function (3.17) with b =0.1833 (2.232) and γ=1.961 (1.418).

JCAP04(2020)001

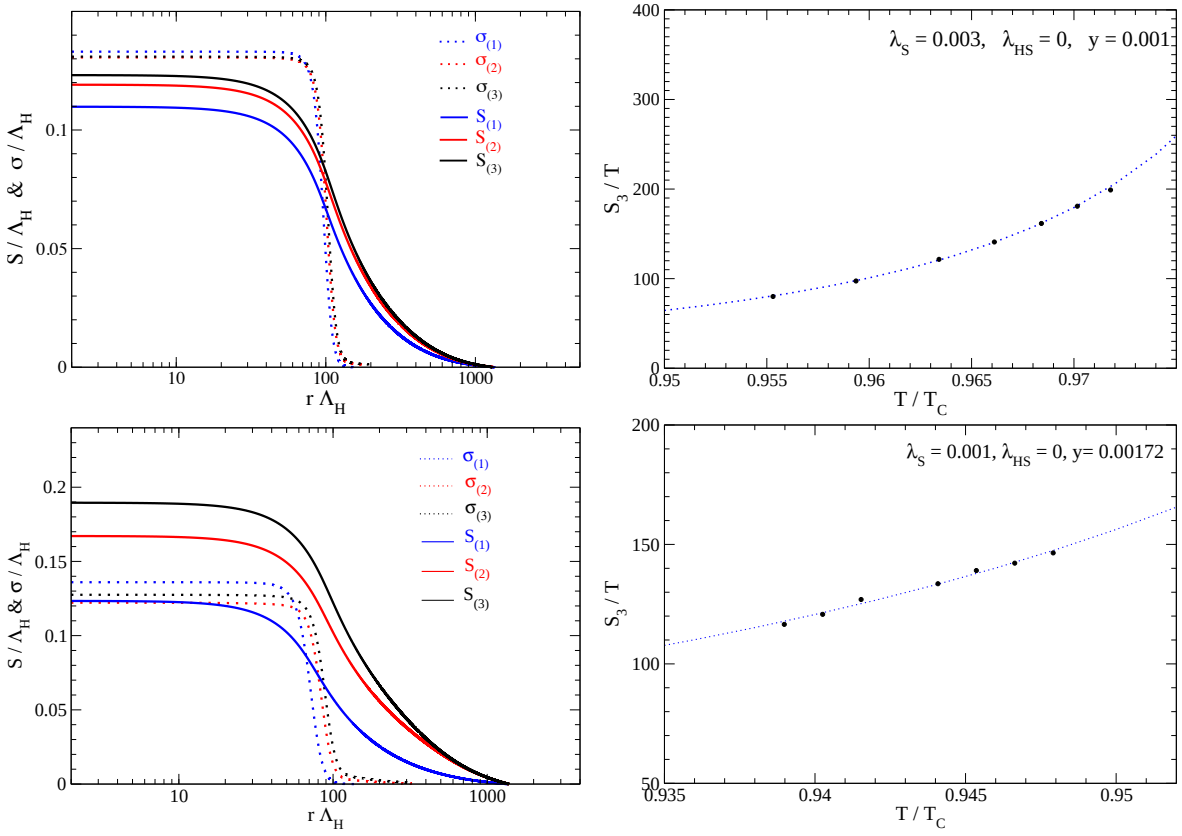

Figure 5. Upper (lower) left: The bounce solutions $\sigma_{(n)}(r)$ and $S_{(n)}(r)$ for $n = 1$ (blue), 2 (red) and 3 (black), where we have used the parameters: $\lambda_S = 0.003\,(0.001)$, $\lambda_{HS} = 0$, $y = 0.001\,(0.00172)$, $T_C/\Lambda_H = 0.0796\,(0.0843)$, $T/\Lambda_H = 0.0769\,(0.0798)$. Upper (lower) right: S_3/T (in the second round) against $x = T/T_C$ with the same λ_S, λ_{HS} and y as in the upper (lower) left panel. The black points are obtained by applying our iterative method, while the blue dotted line is the fitting function defined in eq. (3.17) with $b = 0.1833\,(2.232)$ and $\gamma = 1.961\,(1.418)$.

There is a limitation of our iterative method. As we have discussed in section 3.1, the chiral PT turns into a cross-over type for large y. We have found that our iterative process does not converge for large y even much before the chiral PT turns into a cross-over type. The reason is that a new local minimum, other than the true and false minima, develops near the origin $\sigma = S = 0$. The bounce solution passes near the new local minimum to arrive at the origin, as one can see in figure 6. The depth of the new local minimum becomes deeper and deeper with an increasing value of y, and around a certain value of y the new local minimum starts to affect the iterative method in such a way that the iterative process does not converge. At the moment we are not able to find a bounce solution beyond this value of y.

4 Gravitational wave spectrum

There are three production mechanisms of the stochastic GW background at a strong first-order PT: Bubbles are nucleated and grow, and then the collisions of the bubble walls take place, producing a GW background [58–60, 81–83]. We denote by Ω_φ its contribution to the total GW spectrum $\Omega_{\rm GW}$. After the bubble-wall collisions sound waves surrounding the

JCAP04(2020)001

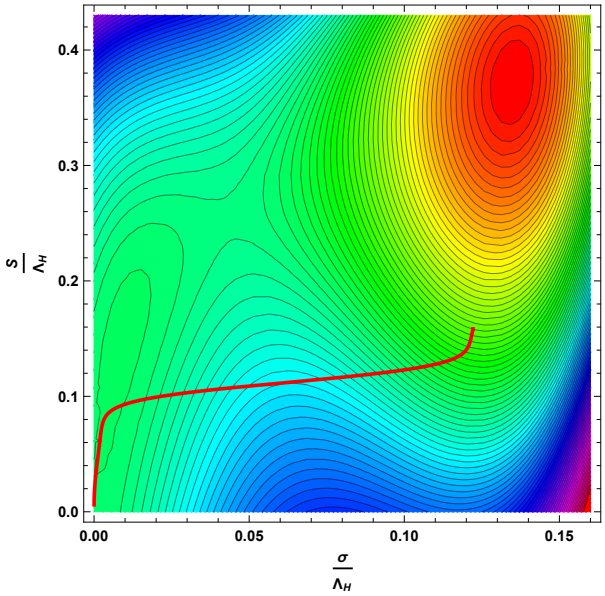

Figure 6. The contour plot of the effective potential $V_{\rm EFF}(S,\sigma,T)/\Lambda_H^4$ at $T/T_C = 0.945$ for $\lambda_S = 0.001$, $\lambda_{HS} = 0$, $y = 0.00172$. The true minimum is located in the upper right corner. A shallow local minimum can be seen on the left side. The red curve is the bounce solution with $S_3/T \simeq 141$.

bubble walls [67, 84–87] and magnetohydrodynamic (MHD) turbulence [88–94] in the plasma become the source of the GW background. Their contributions to $\Omega_{\rm GW}$ are denoted by $\Omega_{\rm sw}$ and $\Omega_{\rm turb}$, respectively:

$$\Omega_{\rm GW}(f)h^2 = [\,\Omega_\varphi(f) + \Omega_{\rm sw}(f) + \Omega_{\rm turb}(f)\,]\,h^2, \tag{4.1}$$

where h is the dimensionless Hubble parameter, and f is the frequency of the GW at present. To calculate $\Omega_{\rm GW}$ for a given model we first have to find out the nucleation temperature T_n. Then we compute the duration time of the first-order PT at $T = T_n$ and the released vacuum energy density at $T = T_n$. The released vacuum energy is indeed the source for the GW energy density, but only its part is effectively used as the source. The corresponding efficiency is expressed by the efficiency coefficients that again depend on the released vacuum energy density. In the following we start by computing $T = T_n$.

4.1 Nucleation temperature T_n

The cosmological tunneling process is quantum mechanical transition from a false vacuum sate to the true vacuum state in the expanding Universe and has been studied in refs. [33, 62, 65, 95, 96]. The probability of the decay rate of the false vacuum per unit volume per unit time at a finite temperature T is given by [65]

$$\Gamma(T) \simeq T^4 \left(\frac{S_3}{2\pi T}\right)^{3/2} \exp(-S_3/T)\,, \tag{4.2}$$

where S_3 is the three dimensional Euclidean action and is given in eq. (3.9) for our model. The first-order PT proceeds via the tunneling process in the expanding Universe, in which the bubbles of the true vacuum are nucleated. Since after each tunneling process we have one bubble nucleation, $\Gamma(T)$ is also the nucleation rate of the bubbles. The nucleation temperature

JCAP04(2020)001

T_n is defined as the temperature, at which one bubble for Hubble time and Hubble volume is nucleated, i.e., $\Gamma(T_n)/H(T_n)^4 = 1$, which leads to the approximate expression [33, 62]

$$\frac{S_3(T_n)}{T_n} \simeq 2\ln\left(\frac{90}{g_*\pi^2}\frac{M_{\rm Pl}^2}{T_n^2}\right), \tag{4.3}$$

where we have ignored the slowly varying factor $(S_3/(2\pi T))^{3/2}$ on the r.h.s. of eq. (4.2), g_* is the relativistic degrees of freedom in the Universe at $T = T_n$, and $M_{\rm Pl} = 2.435 \times 10^{18}\,\text{GeV}$ is the reduced Planck mass. Then the nucleated bubbles expand and collide. Note that the absolute scale of T_n (and also T_C) depends crucially on λ_{HS} and y, because in the absence of both couplings the scale in the hidden sector can be anything; no information about the energy scale in the SM sector, e.g. $m_h \simeq 0.125\,\text{TeV}$, can be transferred to the hidden sector.

4.2 Duration of the phase transition

The temperature T and time t in the expanding Universe is related through

$$\frac{dT}{dt} = -H(t)T\,. \tag{4.4}$$

The nucleation time t_n is the time, at which the temperature T is equal to the nucleation temperature T_n. Since the nucleation time t_n is now defined, we can compute the duration of the phase transition. To this end, we consider the four-dimensional Euclidean action $S_{\rm E}(t) = S_3(T)/T$ and expand it around t_n:

$$S_E(t) = S_E(t_n) - \beta\Delta t + O((\Delta t)^2)\,, \tag{4.5}$$

where $\Delta t = (t - t_n) > 0$. Then the nucleation rate for $t \sim t_n$ can be written as

$$\Gamma(T) \simeq \Gamma(T_n)e^{\beta\Delta t}. \tag{4.6}$$

Clearly, the larger $1/\beta$ is, the longer is the time for which $\Gamma(T)$ stays close to $\Gamma(T_n)$. Therefore, β^{-1} is the duration time and can be computed from [58–60]

$$\beta = -\frac{dS_E}{dt}\bigg|_{t=t_n} = \frac{1}{\Gamma}\frac{d\Gamma}{dt}\bigg|_{t=t_n} = H(t_n)T_n\frac{d}{dT}\left(\frac{S_3}{T}\right)\bigg|_{T=T_n}, \tag{4.7}$$

where eqs. (4.2) and (4.4) are used. This means that we need to compute the derivative of S_3/T, which is a cumbersome task in the presence of many scalar fields involved in the bounce equation like in our case. To overcome this problem we use the fact that S_3/T can be well approximated by the fitting function defined in eq. (3.17). Since b and γ are independent of $x = T/T_C$, we determine them from the actual calculation of S_3/T for some x and obtain β/H from

$$\beta/H = T\frac{d}{dT}\,b(1 - T/T_C)^{-\gamma}\bigg|_{T=T_n} = b\gamma x_n(1-x_n)^{-1-\gamma}\,,\ \text{where } x_n = T_n/T_C\,. \tag{4.8}$$

The quantities, b and γ, do not depend very much on λ_{HS}, because not only they are dimensionless, but also λ_{HS} enters into the chiral PT only through the thermal mass of S as one can see in eq. (3.5). In contrast to this, they and hence β/H depend considerably on y, because it is the origin of the explicit breaking of the chiral symmetry. In figure 7 (left)

JCAP04(2020)001

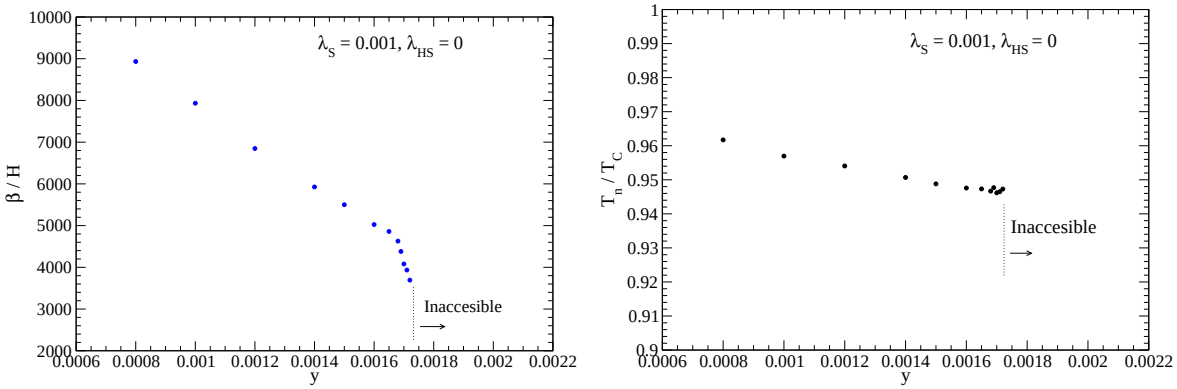

Figure 7. Left: β/H against the Yukawa coupling y for $\lambda_S = 0.001$ and $\lambda_{HS} = 0$, which should be compared with $\beta^{\rm NJL}/H = 1.4 \times 10^4$ [61] (the value without the singlet scalar S). In contrast to β/H, α differs only slightly from the pure NJL value: $g_*\alpha \simeq 3.8$, where it is about 3.2 in the pure NJL case [61]. Beyond $y \gtrsim 0.00172$ (for $\lambda_S = 0.001$), the local minimum on the left side in figure 6 becomes deeper in such a way that the iterative process in solving the coupled differential equations given in (3.12) and (3.13) do not converge, and consequently our method can not be applied. This area in the parameter space is indicated by "inaccessible". Right: The y-dependence of T_n/T_C for $\lambda_S = 0.001$ and $\lambda_{HS} = 0$.

we show β/H for several values of y with λ_S and λ_{HS} fixed at 0.001 and 0, respectively. Since $\beta/H \simeq 1.4 \times 10^4$ in the pure NJL model [61], we see from figure 7 that the larger y is, the more deviation from the pure NJL model we can expect. The right panel shows the y-dependence of T_n/T_C for $\lambda_S = 0.001$ and $\lambda_{HS} = 0$, from which we see that in contrast to β/H the value of T_n/T_C does not change very much as y changes.[8] For $y \gtrsim 0.00172$ our iterative method breaks down (as it is explained in section 3.2), so that we stop at $y = 0.00172$ for this example.

4.3 Released vacuum energy

As we see from figure 7, β/H is large $\sim 10^3$. Therefore, the scalar contribution Ω_φ to the GW spectrum, being proportional to $(\beta/H)^{-2}$, is much more suppressed than the other contributions $\Omega_{\rm sw}$ and $\Omega_{\rm turb}$, because they are proportional to $(\beta/H)^{-1}$ (see eqs. (4.21), (4.24) and (4.27)). Furthermore, as we will see, the turbulence contribution $\Omega_{\rm turb}$ is suppressed, compared with $\Omega_{\rm sw}$, because the relevant GW frequency f is much larger than h_n, the Hubble parameter at T_n, which is red-shifted today. Therefore, we here focus on the sound-wave contribution and follow the treatment of ref. [70]. It should be noted that the definition of α in ref. [70] is not the ratio of the latent heat released at the PT to the radiation energy of the Universe. Instead, they use the trace of the energy momentum tensor of the plasma, leading to

$$\alpha = \frac{1}{\rho_{\rm rad}(T_n)} \left(\Delta V(T_n) - \frac{1}{4} T \frac{\partial \Delta V(T)}{\partial T}\bigg|_{T=T_n} \right) , \tag{4.9}$$

where $\Delta V(T) = V_{\rm EFF}(0,0,T) - V_{\rm EFF}(\langle S\rangle, \langle\sigma\rangle, T)$, and $\rho_{\rm rad}(T) = \pi^2 g_* T^4/30$. According to ref. [70], if the speed of the wall ξ_w is larger than ξ_J, we may identify the vacuum energy den-

[8] β/H computed in ref. [31] does not seem to approach the pure NJL value, $\sim 10^4$, as the Yukawa coupling y goes to zero (see, e.g, the result for the case C in TABLE I and II; $y = 1.07 \times 10^{-4}$ but $\beta/H = 7.15 \times 10^2$.) Therefore, we suspect that the modified path deformation method of ref. [31] to obtain the bounce solution of a coupled system fails to yield trustful results.

JCAP04(2020)001

sity, which enters into the definition of α, with the vacuum energy density outside of the bubble (as we have already done so above), where ξ_J is the wall speed for the Jouguet detonation

$$\xi_J = \frac{\sqrt{\alpha(2+3\alpha)}+1}{\sqrt{3}(1+\alpha)}\,. \tag{4.10}$$

Correspondingly, g_* in $\rho_{\rm rad}$ is the relativistic degrees of freedom in the symmetry phase, which is not necessarily the same as that at the GW production. So, in our case

$$g_* = 106.75 + 1 + 8\times 2 + \frac{7}{8}\times 3\times 3\times 2\times 2 = 155.25\,. \tag{4.11}$$

When calculating the GW spectrum later on, we will be considering an optimistic parameter space given by

$$\lambda_S = 0.001\,,\ \lambda_{HS}\in[0.0001, 0.018]\,,\ y\in[0.0008, 0.00172]\,. \tag{4.12}$$

In this parameter space, α does not change very much:

$$0.0242 \lesssim \alpha \lesssim 0.0250\,. \tag{4.13}$$

4.4 Reduction of the sound-wave contribution

As we mentioned above, the sound-wave contribution $\Omega_{\rm sw}$ will be the most dominant one in our model. The formula for $\Omega_{\rm sw}h^2$ (see eq. (4.24)) has been derived from the numerical simulations for which a long-lasting source of the GW, i.e., $\tau_{\rm sw}H > 1$, is assumed [67], where

$$\tau_{\rm sw} \simeq (8\pi)^{1/3}\frac{\xi_w}{\bar{U}_f\beta} \tag{4.14}$$

is the duration of the sound-wave period, $\bar{U}_f$ is the root-mean four-velocity of the plasma, and ξ_w stands for the speed of the wall (β is defined in eq. (4.8)). That is, $\tau_{\rm sw}H \propto (\beta/H)^{-1}$, so that $\tau_{\rm sw}H > 1$ is unlikely satisfied in our model, because $\beta/H \gtrsim O(10^3)$. In refs. [68, 69] it has been suggested, for the case that $\tau_{\rm sw}H < 1$, to use this quantity as a reduction factor for $\Omega_{\rm sw}$ to take into account the fact that the sound wave is an active GW source only for a period shorter than the Hubble time. Here we follow ref. [68] along with ref. [70] to calculate $\tau_{\rm sw}$ and consider throughout the case of detonations of the plasma motion.

The root-mean four-velocity $\bar{U}_f$ can be calculated from [70]

$$\bar{U}_f^2 = \frac{3}{\xi_w^3}\int_{c_s}^{\xi_w} d\xi \frac{\xi^2 v^2(\xi)}{1-v^2(\xi)}\,, \tag{4.15}$$

where $v(\xi)$ is the velocity profile of the plasma in the frame of the bubble center, and c_s is the speed of sound in the plasma (we assume here $c_s = 1/\sqrt{3}$). The velocity profile $v(\xi)$ satisfies the first-order differential equation [70]

$$\frac{v}{\xi} = \frac{1}{2}\left(\frac{1-v\,\xi}{1-v^2}\right)\left(\frac{\mu^2(\xi,v)}{c_s^2}-1\right)\frac{dv}{d\xi}\,,\ \text{where}\ \mu(\xi,v) = \frac{\xi - v}{1-\xi v}\,. \tag{4.16}$$

To solve the differential equation (4.16) uniquely, we use $v(\xi_w)$ as an initial value, i.e., the plasma speed just behind the wall. Since we focus on the detonations, the plasma in front of the wall is at rest in the bubble center frame, i.e., $v_+ = \xi_w$, where v_+ is the speed of the

JCAP04(2020)001

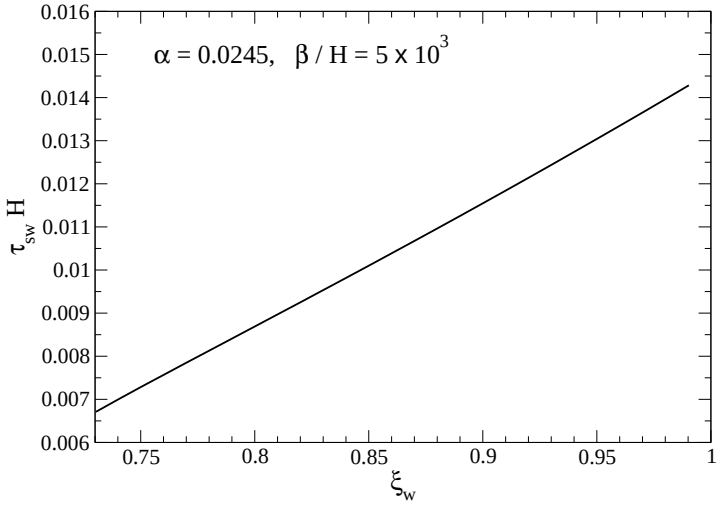

Figure 8. The reduction factor $\tau_{\rm sw}H$ for $\Omega_{\rm sw}$ against the wall speed $\xi_w \geq \xi_J \simeq 0.691$ for $\alpha = 0.0245$ and $\beta/H = 5 \times 10^3$, where $\tau_{\rm sw}$ is defined in (4.14).

plasma in front of the wall in the wall frame (ξ_w is the speed of the wall in the bubble center frame). Therefore, the speed of the plasma just behind the wall in the wall frame, denoted by v_-, can be obtained by the Lorentz transformation

$$-v_- = \frac{v(\xi_w) - \xi_w}{1 - \xi_w v(\xi_w)} \,. \tag{4.17}$$

(The minus sign is introduced, because the plasma velocity in the wall frame has the opposite direction compared with the wall velocity in the bubble center frame.) Eq. (4.17) can be used to obtain

$$v(\xi_w) = \frac{v_+ - v_-}{1 - v_+ v_-} \quad \text{with } v_+ = \xi_w \,, \tag{4.18}$$

where $v_\pm$ are constrained by the matching equations between the plasma sates in front of and behind the wall:

$$\xi_w = v_+ = \frac{1}{1+\alpha}\left[\left(\frac{v_-}{2} + \frac{1}{6v_-}\right) + \left\{\left(\frac{v_-}{2} + \frac{1}{6v_-}\right)^2 + \alpha^2 + \frac{2}{3}\alpha - \frac{1}{3}\right\}^{1/2}\right] . \tag{4.19}$$

So, we obtain v_- from eq. (4.19) for a given set of ξ_w and α and insert it into the r.h.s. of eq. (4.18) to obtain the initial value $v(\xi_w)$. Since the minimum value of v_- is c_s for the detonations to be realized [70], we find that the minimum value of ξ_w is just the Jouguet speed ξ_J defined in eq. (4.10). To obtain an idea on the size of $\tau_{\rm sw}H$, we show $\tau_{\rm sw}H$ in figure 8 as a function of ξ_w ($\geq \xi_J$) for $\alpha = 0.0245$ and $\beta/H = 5 \times 10^3$. As we see from figure 8, the reduction factor for $\Omega_{\rm sw}$ is of order 10^{-2} in our model.

4.5 Gravitational wave spectrum

Now we are in position to present the GW spectrum $\Omega_{\rm GW}$ of our model. As we have argued, the area (4.12) is an optimistic choice of the parameter space, and we expect that $\Omega_{\rm GW}$ will be smaller in other regions of the parameter space. The relativistic degrees of freedom in the expanding Universe enters in the following expressions. It is the relativistic degrees of

JCAP04(2020)001

freedom g'_* at the time, at which the GW background is produced. Therefore, g'_* varies with the time, because the tunneling process takes place for a finite period of time. It is certainly not g_* that is the one in the symmetric phase (4.11) and has been used for the computation of α in eq. (4.9). In the following we assume that g'_* can be approximated by the relativistic degrees of freedom in the broken phase:

$$g'_* = 106.75 + 8 + 1 + 1\,, \tag{4.20}$$

where 8 comes from the NG bosons, and 1 is from σ as well as from S.

Numerical simulations and analytic estimates [58–60, 67, 81–94, 97] of the individual contributions to $\Omega_{\rm GW}$ lead to the following formula:

- Scalar field contribution Ω_φ [83]:

$$h^2\,\Omega_\varphi(f) = 1.67\times 10^{-5}(\beta/H)^{-2}\left(\frac{\kappa_\varphi\alpha}{1+\alpha}\right)^2\left(\frac{100}{g'_*}\right)^{1/3}\left(\frac{0.11\xi_w^3}{0.42+\xi_w^2}\right)S_\varphi(f), \tag{4.21}$$

  where

$$S_\varphi(f) = \frac{3.8(f/f_\varphi)^{2.8}}{1+2.8(f/f_\varphi)^{3.8}} \tag{4.22}$$

  with the peak frequency

$$f_\varphi = 16.5\times 10^{-6}(\beta/H)\left(\frac{0.62}{1.8-0.1\xi_w+\xi_w^2}\right)\left(\frac{T_n}{100\text{ GeV}}\right)\left(\frac{g'_*}{100}\right)^{1/6}\text{Hz}. \tag{4.23}$$

- Sound-wave contribution $\Omega_{\rm sw}$ [84, 85]:

$$h^2\,\Omega_{\rm sw}(f) = (\tau_{\rm sw}H)\,2.65\times 10^{-6}\,(\beta/H)^{-1}\left(\frac{\kappa_{\rm sw}\alpha}{1+\alpha}\right)^2\left(\frac{100}{g'_*}\right)^{1/3}\xi_w S_{\rm sw}(f), \tag{4.24}$$

  where

$$S_{\rm sw}(f) = (f/f_{\rm sw})^3\left(\frac{7}{4+3(f/f_{\rm sw})^2}\right)^{7/2} \tag{4.25}$$

  with the peak frequency

$$f_{\rm sw} = 1.9\times 10^{-5}\xi_w^{-1}(\beta/H)\left(\frac{T_n}{100\text{ GeV}}\right)\left(\frac{g'_*}{100}\right)^{1/6}\text{Hz}. \tag{4.26}$$

  According to refs. [68, 69], the reduction factor $\tau_{\rm sw}H$ (calculated in section 4.4) is multiplied in eq. (4.24).

- MHD turbulence contribution $\Omega_{\rm turb}$ [93]:

$$h^2\,\Omega_{\rm turb}(f) = (1-\tau_{\rm sw}H)\,3.35\times 10^{-4}\,(\beta/H)^{-1}\left(\frac{\kappa_{\rm sw}\alpha}{1+\alpha}\right)^{\frac{3}{2}}\left(\frac{100}{g'_*}\right)^{1/3}\xi_w S_{\rm turb}(f), \tag{4.27}$$

JCAP04(2020)001

where

$$S_{\rm turb}(f) = \frac{(f/f_{\rm turb})^3}{[1+(f/f_{\rm turb})]^{\frac{11}{3}}(1+8\pi f/h_n)} \tag{4.28}$$

with the peak frequency

$$f_{\rm turb} = 2.7\times 10^{-5}\xi_w^{-1}\tilde{\beta}\left(\frac{T_n}{100\ {\rm GeV}}\right)\left(\frac{g'_*}{100}\right)^{1/6}\ {\rm Hz}\,, \tag{4.29}$$

and

$$h_n = 16.5\times 10^{-6}\left(\frac{T_n}{100\ {\rm GeV}}\right)\left(\frac{g'_*}{100}\right)^{1/6}\ {\rm Hz}\,, \tag{4.30}$$

which is the value (redshifted to today) of the Hubble parameter at the production of the GW. We have introduced the enhancement factor $(1-\tau_{\rm sw}H)$ in eq. (4.27) and used the same efficiency coefficient as for the sound-wave contribution [69].

As we have mentioned in various places and we can see now from eq. (4.21), the scalar contribution Ω_φ is, due to $\beta/H \sim 10^3$, about 2 orders of magnitude smaller than $\Omega_{\rm sw}$. Furthermore, the case at hand corresponds to a nonrunaway scenario, in which the friction between the bubbles in the surrounding plasma prevents the acceleration of the bubble expansion [70, 98]. To see this, we estimate α_∞ according to ref. [70]:

$$\alpha_\infty \simeq \frac{30}{24\pi^2 g_* T_n^2}\left[\frac{1}{2}n_f n_c M^2(\langle S\rangle,\langle\sigma\rangle) + M_S^2(\langle S\rangle)\right] \in (0.078, 0.098) \tag{4.31}$$

for the parameter space (4.12), where $M(S,\sigma)$ and $M_S(S)$ are given in eqs. (2.9) and (3.5), respectively. Therefore, $\alpha_\infty < \alpha \simeq 0.024$ (see (4.13)), so that we have a nonrunaway scenario [70] and ignore the scalar contribution (4.21) in the following discussion.

We use the efficient coefficient $\kappa_{\rm sw}$ given in ref. [70] for $\Omega_{\rm sw}$ and also for $\Omega_{\rm turb}$:

$$\kappa_{\rm sw}(\xi_w \gtrsim \xi_J) \simeq \frac{\chi_J^3\,(\xi_J/\xi_w)^{5/2}\,\kappa_C\kappa_D}{(\chi_J^3-\chi_w^3)\,\xi_J^{5/2}\kappa_C + \chi_w^3\kappa_D}\,, \tag{4.32}$$

where

$$\begin{aligned} &\chi_J = \xi_J - 1\,,\ \chi_w = \xi_w - 1\,,\\ &\kappa_C \simeq \frac{\alpha^{1/2}}{0.135+0.98^{1/2}+\alpha}\,,\quad \kappa_D \simeq \frac{\alpha}{0.73+0.083\,\alpha^{1/2}+\alpha}\,, \end{aligned} \tag{4.33}$$

and ξ_J is given in eq. (4.10). Although $\Omega_{\rm sw}$ is reduced by the reduction factor $\tau_{\rm sw}H$ and $\Omega_{\rm turb}$ is enhanced by $(1-\tau_{\rm sw}H)$ and also by the identification $\kappa_{\rm turb} = \kappa_{\rm sw}$, the turbulence contribution $\Omega_{\rm turb}$ is about one order of magnitude smaller than $\Omega_{\rm sw}$, because $f_{\rm turb}/h_n \sim \beta/H \sim 10^3$ that is in the denominator of eq. (4.28); $(f_{\rm turb}/h_n)^{-1}/(\tau_{\rm sw}H) \sim 0.1$.

As we see from eq. (4.26) the scale of the GW frequency is fixed by the nucleation temperature T_n. Note that the absolute scale of the critical temperature T_C and hence T_n is fixed through the coupling with the SM sector, i.e., λ_{HS} and y. In the left panel of figure 9 we show T_C [TeV] and $f_{\rm sw}$ [Hz] against λ_{HS}. Obviously, the smaller λ_{HS} is, the larger is Λ_H

JCAP04(2020)001

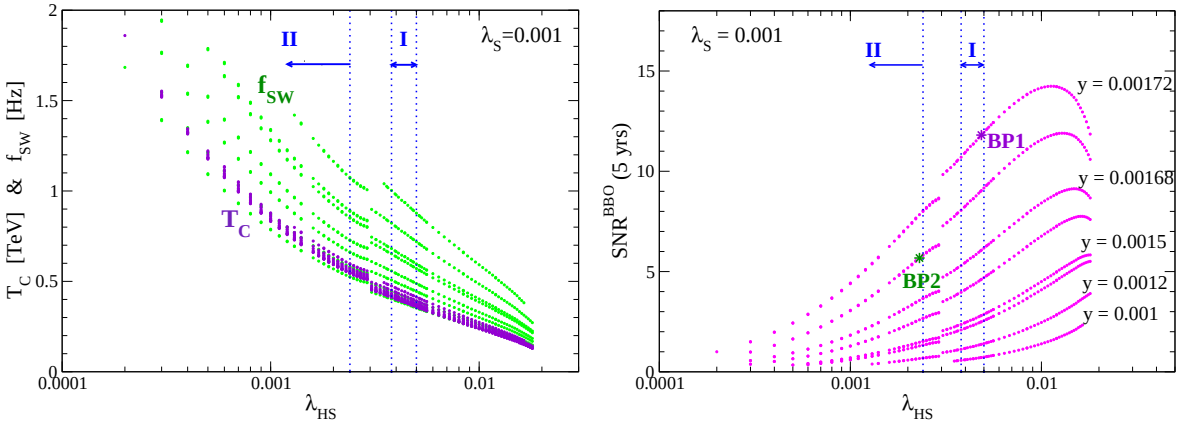

Figure 9. Left: The critical temperature T_C [TeV] (purple) and the peak frequency of the sound-wave contribution $f_{\rm sw}$ [Hz] (green) against λ_{HS}. The area I and II are allowed by LHC (see figure 1). Right: $\mathrm{SNR}^{\rm BBO}$ against λ_{HS} with five years observation. The $\mathrm{SNR}^{\rm BBO}$ (5 yrs) of the benchmark points, BP1(purple star) and BP2 (green star), are also plotted.

(the scale of the hidden sector), and consequently higher T_C and $f_{\rm sw}$. The band of $f_{\rm sw}$ is wider than that of T_C, because β/H depends on y (see figure 7) more than T_C does. As we also see from this figure that the GW frequencies in our model are $\gtrsim 0.3$ Hz, which can be covered by DECIGO [72–74] and BBO [75–77].

We calculate the SNR according to ref. [71],

$$\mathrm{SNR} = \sqrt{2t_{\rm obs}\int_{f_{\rm min}}^{f_{\rm max}} df\left[\frac{\Omega_{\rm GW}(f)\,h^2}{\Omega_{\rm noise}(f)\,h^2}\right]^2}\,, \tag{4.34}$$

where $t_{\rm obs}$ stands for the duration of an observation in seconds, and $(f_{\rm min}, f_{\rm max})$ is the frequency range of a given experiment. The quantity $\Omega_{\rm noise}(f)\,h^2$ represents the effective strain noise power spectral density for a given detector network, expressed as energy density parameter [99]. For the space-based observatories mentioned above, we adopt the strain noise power spectral densities from refs. [100–102]. (We use the sky-averaged sensitivity [101].) The result,[9] SNR against λ_{HS} for BBO, is shown in the right panel of figure 9,[10] where we assume that $t_{\rm obs} = 5$ years and the speed of the wall ξ_w is equal to the Jouguet speed ξ_J given in eq. (4.10). The $\mathrm{SNR}^{\rm BBO}$ (5 yrs) of the benchmark points, BP1 and BP2 defined in (2.21), are 11.8 and 5.7, respectively, while for DECIGO we find $\mathrm{SNR}^{\rm DECIGO}$ (5 yrs) = 1.1 and 0.5, respectively. Therefore, there is a good chance that the GW signals of our model can be detected by BBO, where the area I and II are allowed by LHC (see figure 1).

In the left panel of figure 10 we present the GW spectra for BP1 (purple) and BP2 (green) with $\xi_w = \xi_J$, which should be compared with the power-law-integrated sensitivity [71] of BBO (red dashed curve) and DECIGO (blue dashed curve), where we assume that the threshold SNR is 5 ($\rho_{\rm thr} = 5$) with five years observation for both detectors. Since a part of the spectral curves for BP1 and BP2 runs over the sensitivity curve of BBO, we see once again that their signals could be detected at BBO, while for DECIGO it would be very difficult. For comparison we also present the GW spectra (dotted purple and green

[9] The SNR is computed including the turbulence contribution.

[10] The effect of unresolvable astrophysical foregrounds from black hole, neutron star and white dwarf mergers on the signal significance are ignored.

JCAP04(2020)001

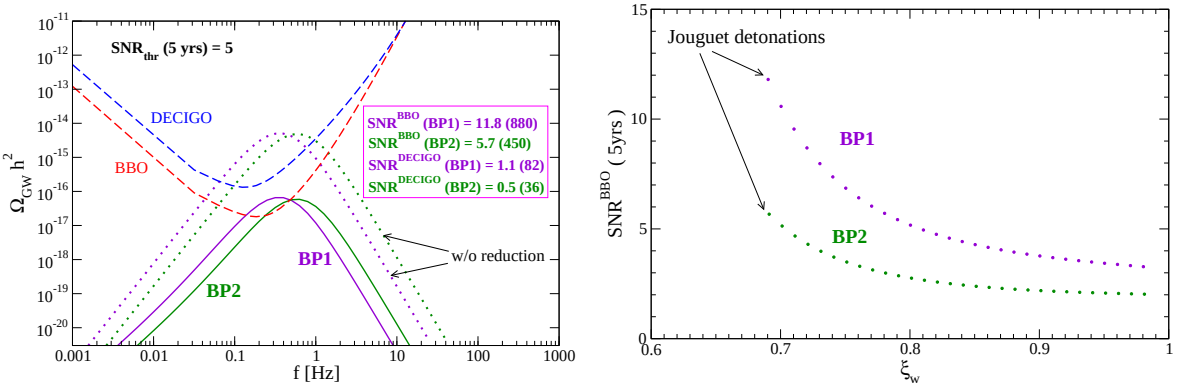

Figure 10. Left: The GW spectrum for the benchmark points BP1 (purple), BP2 (green) and the power-law-integrated sensitivity of BBO (red dashed curve) as well as DECIGO (blue dashed curve), where we assume that the threshold SNR is 5 ($\rho_{\rm thr} = 5$) with five years observation for both detectors. The GW spectrum is computed including the turbulence contribution, which is about one order of magnitude smaller than that of the sound-wave contribution. The dotted purple and green lines present, respectively, the GW spectrum of BP1 and BP2, for which the reduction factor $\tau_{\rm sw}H$ due to the short sound-wave period is ignored. Right: The ξ_w dependence of $\mathrm{SNR}^{\rm BBO}$ (5 yrs). The Jouguet speed ξ_J is the minimum speed of ξ_w for detonations. At this speed the SNR becomes maximal.

lines), which we obtain without the reduction factor $\tau_{\rm sw}H$. We see a difference of 2 orders of magnitude, whose origin is nothing but $\tau_{\rm sw}H \sim 10^{-2}$.

As the last task we consider the dependence of the wall speed ξ_w, because we have assumed so far that it is equal to the Jouguet speed ξ_J. In the right panel of figure 10 we show the ξ_w dependence of $\mathrm{SNR}^{\rm BBO}$ (5 yrs). In fact, $\mathrm{SNR}^{\rm BBO}$ (5 yrs) assumes the maximal value at $\xi_w = \xi_J$, which follows from the fact that the reduction factor $\tau_{\rm sw}H$ decreases as ξ_w increases (see figure 8). But there is still a sufficient range in the parameter space, in which the detectability threshold is exceeded.

5 Summary and conclusion

In this paper we have studied the stochastic GW background produced at the cosmological chiral PT in a conformal extension of the SM [21, 22] and extended the analysis of ref. [31]. In particular, we have re-calculated β/H, because β/H in ref. [31] does not approach the pure NJL value, $\sim 10^4$, as the Yukawa coupling y decreases and for this reason we have suspected that the modified path deformation method of ref. [31] to obtain the bounce solution of a coupled system fails to yield trustful results.

Therefore, we have adopted an iterative method (with a reasonable convergence property) and found that S_3/T can be fitted with a simple function (3.17). Using this fitting function for the determination of β/H we have obtained $\beta/H \simeq (4-9)\times 10^3$ in the optimistic parameter space. We also have found that the benchmark point values of β/H presented in ref. [31] are about one order of magnitude smaller than those calculated by using the new method.

There are, in the $\mathrm{SU}(3)_V$ flavor symmetry limit, five independent parameters, λ_H, λ_S, λ_{HS}, y and g_H (or the hidden sector scale Λ_H), where effectively two of them are used to obtain $m_h = 125\,\mathrm{GeV}$ and $\langle h\rangle = 246\,\mathrm{GeV}$. We have systematically narrowed the parameter space, giving smaller values of β/H than that of the pure NJL model and hence larger (dimensionless) spectral GW energy density $\Omega_{\rm GW}$. Obviously, $\Omega_{\rm GW}$ will be smaller in other

JCAP04(2020)001

regions of the parameter space. In this optimistic parameter space (with $\lambda_S \sim 10^{-3}$) the singlet scalar S can become as light as the Higgs h, and therefore we have taken into account the LHC constraint on their mixing: There are two allowed regions for $\lambda_S = 0.001$ that are denoted by I (for $m_S < m_h$) and II (for $m_S > m_h$). We remark that for this optimistic parameter space in the $\mathrm{SU}(3)_V$ flavor symmetry limit no realistic DM relic abundance can be obtained because the resonant condition ($m_S \simeq 2m_{\mathrm{DM}}$) in the s-channel of the DM annihilation can not be realized [17]. (In the model studied in ref. [31] the flavor group $\mathrm{SU}(3)_V$ is unbroken and the hidden fermions have no $\mathrm{U}(1)_Y$ charge.) This is why we have considered the model with a finite $\mathrm{U}(1)_Y$ charge for the hidden fermions and have explicitly broken $\mathrm{SU}(3)_V$ down to $\mathrm{SU}(2)_V \times \mathrm{U}(1)$ to apply the mechanism of ref. [22] to obtain a realistic DM relic abundance. But for the analyses of the GW background spectrum we have considered the $\mathrm{SU}(3)_V$ limit, because it is only marginally broken and we would have had to deal with three variables (instead of two) to find a bounce solution.

The fact, $\beta/H \simeq (4-9) \times 10^3$, implies a short duration time of the first-order chiral PT, much shorter than the Hubble time, and consequently a short sound wave period τ_{sw} as an active GW source; $\tau_{\mathrm{sw}} H \sim 10^{-2}$. Then following refs. [68, 69] we have used $\tau_{\mathrm{sw}} H$ as the reduction factor for the sound wave contribution Ω_{sw}, which is nevertheless the most dominant contribution to Ω_{GW}. We have evaluated the SNR for DECIGO and BBO and found that $\mathrm{SNR}^{\mathrm{DECIGO}} \lesssim 1.2$ and $\mathrm{SNR}^{\mathrm{BBO}} \lesssim 12.0$ with five years observation, from which we conclude that the GW signal predicted by the model in the optimistic case could be detected at BBO.[11]

At last we recall that the results obtained by using effective theory methods to study the GWs produced at a first-order PT in strong-interacting QCD-like theories agree with each other only qualitatively [61] and for a more precise determination of the GWs we need first-principle calculations (like lattice simulations) which may become available in future [104].

Acknowledgments

We thank Alexander J. Helmboldt and Susan van der Woude for useful discussions. J.K. thanks for kind hospitality at the Max-Planck-Institute for Nuclear Physics, Heidelberg, where a part of this work has been done. The work of M.A. is supported in part by the Japan Society for the Promotion of Sciences Grant-in-Aid for Scientific Research (Grant No. 17K05412). J.K. is partially supported by the Grant-in-Aid for Scientific Research (C) from the Japan Society for Promotion of Science (Grant No.19K03844).

References

[1] M. Lindner, *Conformal extensions of the Standard Model*, in *Particle Astrophysics and Cosmology Including Fundamental InteraCtions (PACIFIC 2019), Moore, French Polynesia, September 1–6, 2019*, https://conferences.pa.ucla.edu/pacific-2019/talks/lindner.pdf.

[2] G. Ross, *Beyond the Standard Model*, *Phys. Atom. Nucl.* **79** (2016) 1445 [INSPIRE].

[3] M. Holthausen, K.S. Lim and M. Lindner, *Planck scale Boundary Conditions and the Higgs Mass*, *JHEP* **02** (2012) 037 [arXiv:1112.2415] [INSPIRE].

[11] With a new sensitivity introduced in ref. ([103]) the detectability may increase.

JCAP04(2020)001

[4] F. Bezrukov, M.Yu. Kalmykov, B.A. Kniehl and M. Shaposhnikov, *Higgs Boson Mass and New Physics*, *JHEP* **10** (2012) 140 [arXiv:1205.2893] [INSPIRE].

[5] G. Degrassi et al., *Higgs mass and vacuum stability in the Standard Model at NNLO*, *JHEP* **08** (2012) 098 [arXiv:1205.6497] [INSPIRE].

[6] D. Buttazzo et al., *Investigating the near-criticality of the Higgs boson*, *JHEP* **12** (2013) 089 [arXiv:1307.3536] [INSPIRE].

[7] F. Wilczek, *Mass without mass. I: Most of matter*, *Phys. Today* **52** (1999) 11.

[8] S.R. Coleman and E.J. Weinberg, *Radiative Corrections as the Origin of Spontaneous Symmetry Breaking*, *Phys. Rev.* **D 7** (1973) 1888 [INSPIRE].

[9] C.G. Callan Jr., *Broken scale invariance in scalar field theory*, *Phys. Rev.* **D 2** (1970) 1541 [INSPIRE].

[10] K. Symanzik, *Small distance behavior in field theory and power counting*, *Commun. Math. Phys.* **18** (1970) 227 [INSPIRE].

[11] A.S. Kronfeld, *Lattice Gauge Theory and the Origin of Mass*, in *100 Years of Subatomic Physics*, E.M. Henley and S.D. Ellis eds., (2013), pp. 493–518, arXiv:1209.3468 [INSPIRE].

[12] Y. Nambu, *Axial vector current conservation in weak interactions*, *Phys. Rev. Lett.* **4** (1960) 380 [INSPIRE].

[13] Y. Nambu and G. Jona-Lasinio, *Dynamical Model of Elementary Particles Based on an Analogy with Superconductivity. 1.*, *Phys. Rev.* **122** (1961) 345 [INSPIRE].

[14] Y. Nambu and G. Jona-Lasinio, *Dynamical model of elementary particles based on an analogy with superconductivity. II*, *Phys. Rev.* **124** (1961) 246 [INSPIRE].

[15] T. Hur and P. Ko, *Scale invariant extension of the standard model with strongly interacting hidden sector*, *Phys. Rev. Lett.* **106** (2011) 141802 [arXiv:1103.2571] [INSPIRE].

[16] M. Heikinheimo, A. Racioppi, M. Raidal, C. Spethmann and K. Tuominen, *Physical Naturalness and Dynamical Breaking of Classical Scale Invariance*, *Mod. Phys. Lett.* **A 29** (2014) 1450077 [arXiv:1304.7006] [INSPIRE].

[17] M. Holthausen, J. Kubo, K.S. Lim and M. Lindner, *Electroweak and Conformal Symmetry Breaking by a Strongly Coupled Hidden Sector*, *JHEP* **12** (2013) 076 [arXiv:1310.4423] [INSPIRE].

[18] J. Kubo, K.S. Lim and M. Lindner, *Electroweak Symmetry Breaking via QCD*, *Phys. Rev. Lett.* **113** (2014) 091604 [arXiv:1403.4262] [INSPIRE].

[19] J. Kubo and M. Yamada, *Genesis of electroweak and dark matter scales from a bilinear scalar condensate*, *Phys. Rev.* **D 93** (2016) 075016 [arXiv:1505.05971] [INSPIRE].

[20] H. Hatanaka, D.-W. Jung and P. Ko, *AdS/QCD approach to the scale-invariant extension of the standard model with a strongly interacting hidden sector*, *JHEP* **08** (2016) 094 [arXiv:1606.02969] [INSPIRE].

[21] J. Kubo, K.S. Lim and M. Lindner, *Gamma-ray Line from Nambu-Goldstone Dark Matter in a Scale Invariant Extension of the Standard Model*, *JHEP* **09** (2014) 016 [arXiv:1405.1052] [INSPIRE].

[22] Y. Ametani, M. Aoki, H. Goto and J. Kubo, *Nambu-Goldstone Dark Matter in a Scale Invariant Bright Hidden Sector*, *Phys. Rev.* **D 91** (2015) 115007 [arXiv:1505.00128] [INSPIRE].

[23] PLANCK collaboration, *Planck 2018 results. VI. Cosmological parameters*, arXiv:1807.06209 [INSPIRE].

JCAP04(2020)001

[24] J. Kubo, M. Lindner, K. Schmitz and M. Yamada, *Planck mass and inflation as consequences of dynamically broken scale invariance*, *Phys. Rev.* **D 100** (2019) 015037 [arXiv:1811.05950] [INSPIRE].

[25] T. Bhattacharya et al., *QCD Phase Transition with Chiral Quarks and Physical Quark Masses*, *Phys. Rev. Lett.* **113** (2014) 082001 [arXiv:1402.5175] [INSPIRE].

[26] R.D. Pisarski and F. Wilczek, *Remarks on the Chiral Phase Transition in Chromodynamics*, *Phys. Rev.* **D 29** (1984) 338 [INSPIRE].

[27] C. DeTar and U.M. Heller, *QCD Thermodynamics from the Lattice*, *Eur. Phys. J.* **A 41** (2009) 405 [arXiv:0905.2949] [INSPIRE].

[28] H.B. Meyer, *QCD at non-zero temperature from the lattice*, PoS(LATTICE 2015)014 [arXiv:1512.06634] [INSPIRE].

[29] X.-Y. Jin, Y. Kuramashi, Y. Nakamura, S. Takeda and A. Ukawa, *Critical point phase transition for finite temperature 3-flavor QCD with non-perturbatively O(a) improved Wilson fermions at $N_t = 10$*, *Phys. Rev.* **D 96** (2017) 034523 [arXiv:1706.01178] [INSPIRE].

[30] J. Kubo and M. Yamada, *Scale and electroweak first-order phase transitions*, *PTEP* **2015** (2015) 093B01 [arXiv:1506.06460] [INSPIRE].

[31] M. Aoki, H. Goto and J. Kubo, *Gravitational Waves from Hidden QCD Phase Transition*, *Phys. Rev.* **D 96** (2017) 075045 [arXiv:1709.07572] [INSPIRE].

[32] P. Schwaller, *Gravitational Waves from a Dark Phase Transition*, *Phys. Rev. Lett.* **115** (2015) 181101 [arXiv:1504.07263] [INSPIRE].

[33] E. Witten, *Cosmic Separation of Phases*, *Phys. Rev.* **D 30** (1984) 272 [INSPIRE].

[34] M. Maggiore, *Gravitational wave experiments and early universe cosmology*, *Phys. Rept.* **331** (2000) 283 [gr-qc/9909001] [INSPIRE].

[35] P. Binetruy, A. Bohe, C. Caprini and J.-F. Dufaux, *Cosmological Backgrounds of Gravitational Waves and eLISA/NGO: Phase Transitions, Cosmic Strings and Other Sources*, *JCAP* **06** (2012) 027 [arXiv:1201.0983] [INSPIRE].

[36] N. Seto and J. Yokoyama, *Probing the equation of state of the early universe with a space laser interferometer*, *J. Phys. Soc. Jap.* **72** (2003) 3082 [gr-qc/0305096] [INSPIRE].

[37] S. Kuroyanagi, T. Chiba and N. Sugiyama, *Precision calculations of the gravitational wave background spectrum from inflation*, *Phys. Rev.* **D 79** (2009) 103501 [arXiv:0804.3249] [INSPIRE].

[38] S. Schettler, T. Boeckel and J. Schaffner-Bielich, *Imprints of the QCD Phase Transition on the Spectrum of Gravitational Waves*, *Phys. Rev.* **D 83** (2011) 064030 [arXiv:1010.4857] [INSPIRE].

[39] T. Boeckel, S. Schettler and J. Schaffner-Bielich, *The Cosmological QCD Phase Transition Revisited*, *Prog. Part. Nucl. Phys.* **66** (2011) 266 [arXiv:1012.3342] [INSPIRE].

[40] K. Saikawa and S. Shirai, *Primordial gravitational waves, precisely: The role of thermodynamics in the Standard Model*, *JCAP* **05** (2018) 035 [arXiv:1803.01038] [INSPIRE].

[41] F. Hajkarim, J. Schaffner-Bielich, S. Wystub and M.M. Wygas, *Effects of the QCD Equation of State and Lepton Asymmetry on Primordial Gravitational Waves*, *Phys. Rev.* **D 99** (2019) 103527 [arXiv:1904.01046] [INSPIRE].

[42] LIGO Scientific and Virgo collaborations, *Observation of Gravitational Waves from a Binary Black Hole Merger*, *Phys. Rev. Lett.* **116** (2016) 061102 [arXiv:1602.03837] [INSPIRE].

JCAP04(2020)001

[43] LIGO Scientific and Virgo collaborations, *GW170817: Observation of Gravitational Waves from a Binary Neutron Star Inspiral*, *Phys. Rev. Lett.* **119** (2017) 161101 [arXiv:1710.05832] [INSPIRE].

[44] LIGO Scientific et al. collaborations, *Multi-messenger Observations of a Binary Neutron Star Merger*, *Astrophys. J.* **848** (2017) L12 [arXiv:1710.05833] [INSPIRE].

[45] T. Konstandin and G. Servant, *Cosmological Consequences of Nearly Conformal Dynamics at the TeV scale*, *JCAP* **12** (2011) 009 [arXiv:1104.4791] [INSPIRE].

[46] K. Hashino, S. Kanemura and Y. Orikasa, *Discriminative phenomenological features of scale invariant models for electroweak symmetry breaking*, *Phys. Lett.* **B 752** (2016) 217 [arXiv:1508.03245] [INSPIRE].

[47] K. Tsumura, M. Yamada and Y. Yamaguchi, *Gravitational wave from dark sector with dark pion*, *JCAP* **07** (2017) 044 [arXiv:1704.00219] [INSPIRE].

[48] L. Marzola, A. Racioppi and V. Vaskonen, *Phase transition and gravitational wave phenomenology of scalar conformal extensions of the Standard Model*, *Eur. Phys. J.* **C 77** (2017) 484 [arXiv:1704.01034] [INSPIRE].

[49] R. Jinno and M. Takimoto, *Probing a classically conformal B-L model with gravitational waves*, *Phys. Rev.* **D 95** (2017) 015020 [arXiv:1604.05035] [INSPIRE].

[50] T. Prokopec, J. Rezacek and B. Świeżewska, *Gravitational waves from conformal symmetry breaking*, *JCAP* **02** (2019) 009 [arXiv:1809.11129] [INSPIRE].

[51] K. Hashino, R. Jinno, M. Kakizaki, S. Kanemura, T. Takahashi and M. Takimoto, *Selecting models of first-order phase transitions using the synergy between collider and gravitational-wave experiments*, *Phys. Rev.* **D 99** (2019) 075011 [arXiv:1809.04994] [INSPIRE].

[52] V. Brdar, A.J. Helmboldt and J. Kubo, *Gravitational Waves from First-Order Phase Transitions: LIGO as a Window to Unexplored Seesaw Scales*, *JCAP* **02** (2019) 021 [arXiv:1810.12306] [INSPIRE].

[53] K. Miura, H. Ohki, S. Otani and K. Yamawaki, *Gravitational Waves from Walking Technicolor*, *JHEP* **10** (2019) 194 [arXiv:1811.05670] [INSPIRE].

[54] C. Marzo, L. Marzola and V. Vaskonen, *Phase transition and vacuum stability in the classically conformal B-L model*, *Eur. Phys. J.* **C 79** (2019) 601 [arXiv:1811.11169] [INSPIRE].

[55] D. Croon, R. Houtz and V. Sanz, *Dynamical Axions and Gravitational Waves*, *JHEP* **07** (2019) 146 [arXiv:1904.10967] [INSPIRE].

[56] D.-C. Dai and D. Stojkovic, *Primordial scalar gravitational waves produced at the QCD phase transition due to the trace anomaly*, *Class. Quant. Grav.* **36** (2019) 145004 [arXiv:1905.05850] [INSPIRE].

[57] A. Mohamadnejad, *Gravitational waves from scale-invariant vector dark matter model: Probing below the neutrino-floor*, *Eur. Phys. J.* **C 80** (2020) 197 [arXiv:1907.08899] [INSPIRE].

[58] A. Kosowsky, M.S. Turner and R. Watkins, *Gravitational radiation from colliding vacuum bubbles*, *Phys. Rev.* **D 45** (1992) 4514 [INSPIRE].

[59] A. Kosowsky, M.S. Turner and R. Watkins, *Gravitational waves from first order cosmological phase transitions*, *Phys. Rev. Lett.* **69** (1992) 2026 [INSPIRE].

[60] A. Kosowsky and M.S. Turner, *Gravitational radiation from colliding vacuum bubbles: envelope approximation to many bubble collisions*, *Phys. Rev.* **D 47** (1993) 4372 [astro-ph/9211004] [INSPIRE].

JCAP04(2020)001

[61] A.J. Helmboldt, J. Kubo and S. van der Woude, *Observational prospects for gravitational waves from hidden or dark chiral phase transitions*, *Phys. Rev.* **D 100** (2019) 055025 [arXiv:1904.07891] [INSPIRE].

[62] C.J. Hogan, *Nucleation of cosmological phase transitions*, *Phys. Lett.* **133B** (1983) 172 [INSPIRE].

[63] A. Falkowski, C. Gross and O. Lebedev, *A second Higgs from the Higgs portal*, *JHEP* **05** (2015) 057 [arXiv:1502.01361] [INSPIRE].

[64] T. Robens and T. Stefaniak, *LHC Benchmark Scenarios for the Real Higgs Singlet Extension of the Standard Model*, *Eur. Phys. J.* **C 76** (2016) 268 [arXiv:1601.07880] [INSPIRE].

[65] A.D. Linde, *Decay of the False Vacuum at Finite Temperature*, *Nucl. Phys.* **B 216** (1983) 421 [*Erratum ibid.* **B 223** (1983) 544] [INSPIRE].

[66] C.L. Wainwright, *CosmoTransitions: Computing Cosmological Phase Transition Temperatures and Bubble Profiles with Multiple Fields*, *Comput. Phys. Commun.* **183** (2012) 2006 [arXiv:1109.4189] [INSPIRE].

[67] M. Hindmarsh, S.J. Huber, K. Rummukainen and D.J. Weir, *Shape of the acoustic gravitational wave power spectrum from a first order phase transition*, *Phys. Rev.* **D 96** (2017) 103520 [arXiv:1704.05871] [INSPIRE].

[68] J. Ellis, M. Lewicki and J.M. No, *On the Maximal Strength of a First-Order Electroweak Phase Transition and its Gravitational Wave Signal*, arXiv:1809.08242 [INSPIRE].

[69] J. Ellis, M. Lewicki, J.M. No and V. Vaskonen, *Gravitational wave energy budget in strongly supercooled phase transitions*, *JCAP* **06** (2019) 024 [arXiv:1903.09642] [INSPIRE].

[70] J.R. Espinosa, T. Konstandin, J.M. No and G. Servant, *Energy Budget of Cosmological First-order Phase Transitions*, *JCAP* **06** (2010) 028 [arXiv:1004.4187] [INSPIRE].

[71] E. Thrane and J.D. Romano, *Sensitivity curves for searches for gravitational-wave backgrounds*, *Phys. Rev.* **D 88** (2013) 124032 [arXiv:1310.5300] [INSPIRE].

[72] N. Seto, S. Kawamura and T. Nakamura, *Possibility of direct measurement of the acceleration of the universe using 0.1-Hz band laser interferometer gravitational wave antenna in space*, *Phys. Rev. Lett.* **87** (2001) 221103 [astro-ph/0108011] [INSPIRE].

[73] S. Kawamura et al., *The Japanese space gravitational wave antenna DECIGO*, *Class. Quant. Grav.* **23** (2006) S125 [INSPIRE].

[74] S. Kawamura et al., *The Japanese space gravitational wave antenna: DECIGO*, *Class. Quant. Grav.* **28** (2011) 094011 [INSPIRE].

[75] S. Phinney et al., *The Big Bang Observer: Direct detection of gravitational waves from the birth of the Universe to the Present*, NASA Mission Concept Study (2004).

[76] N.J. Cornish and J. Crowder, *LISA data analysis using MCMC methods*, *Phys. Rev.* **D 72** (2005) 043005 [gr-qc/0506059] [INSPIRE].

[77] V. Corbin and N.J. Cornish, *Detecting the cosmic gravitational wave background with the big bang observer*, *Class. Quant. Grav.* **23** (2006) 2435 [gr-qc/0512039] [INSPIRE].

[78] T. Kunihiro and T. Hatsuda, *A Selfconsistent Mean Field Approach to the Dynamical Symmetry Breaking: The Effective Potential of the Nambu-Jona-Lasinio Model*, *Prog. Theor. Phys.* **71** (1984) 1332 [INSPIRE].

[79] T. Hatsuda and T. Kunihiro, *QCD phenomenology based on a chiral effective Lagrangian*, *Phys. Rept.* **247** (1994) 221 [hep-ph/9401310] [INSPIRE].

[80] R. Apreda, M. Maggiore, A. Nicolis and A. Riotto, *Gravitational waves from electroweak phase transitions*, *Nucl. Phys.* **B 631** (2002) 342 [gr-qc/0107033] [INSPIRE].

JCAP04(2020)001

[81] M. Kamionkowski, A. Kosowsky and M.S. Turner, *Gravitational radiation from first order phase transitions*, *Phys. Rev.* **D 49** (1994) 2837 [astro-ph/9310044] [INSPIRE].

[82] C. Caprini, R. Durrer and G. Servant, *Gravitational wave generation from bubble collisions in first-order phase transitions: An analytic approach*, *Phys. Rev.* **D 77** (2008) 124015 [arXiv:0711.2593] [INSPIRE].

[83] S.J. Huber and T. Konstandin, *Gravitational Wave Production by Collisions: More Bubbles*, *JCAP* **09** (2008) 022 [arXiv:0806.1828] [INSPIRE].

[84] M. Hindmarsh, S.J. Huber, K. Rummukainen and D.J. Weir, *Gravitational waves from the sound of a first order phase transition*, *Phys. Rev. Lett.* **112** (2014) 041301 [arXiv:1304.2433] [INSPIRE].

[85] M. Hindmarsh, S.J. Huber, K. Rummukainen and D.J. Weir, *Numerical simulations of acoustically generated gravitational waves at a first order phase transition*, *Phys. Rev.* **D 92** (2015) 123009 [arXiv:1504.03291] [INSPIRE].

[86] J.T. Giblin Jr. and J.B. Mertens, *Vacuum Bubbles in the Presence of a Relativistic Fluid*, *JHEP* **12** (2013) 042 [arXiv:1310.2948] [INSPIRE].

[87] J.T. Giblin and J.B. Mertens, *Gravitional radiation from first-order phase transitions in the presence of a fluid*, *Phys. Rev.* **D 90** (2014) 023532 [arXiv:1405.4005] [INSPIRE].

[88] A. Kosowsky, A. Mack and T. Kahniashvili, *Gravitational radiation from cosmological turbulence*, *Phys. Rev.* **D 66** (2002) 024030 [astro-ph/0111483] [INSPIRE].

[89] C. Caprini and R. Durrer, *Gravitational waves from stochastic relativistic sources: Primordial turbulence and magnetic fields*, *Phys. Rev.* **D 74** (2006) 063521 [astro-ph/0603476] [INSPIRE].

[90] T. Kahniashvili, L. Campanelli, G. Gogoberidze, Y. Maravin and B. Ratra, *Gravitational Radiation from Primordial Helical Inverse Cascade MHD Turbulence*, *Phys. Rev.* **D 78** (2008) 123006 [*Erratum ibid.* **D 79** (2009) 109901] [arXiv:0809.1899] [INSPIRE].

[91] T. Kahniashvili, A. Kosowsky, G. Gogoberidze and Y. Maravin, *Detectability of Gravitational Waves from Phase Transitions*, *Phys. Rev.* **D 78** (2008) 043003 [arXiv:0806.0293] [INSPIRE].

[92] T. Kahniashvili, L. Kisslinger and T. Stevens, *Gravitational Radiation Generated by Magnetic Fields in Cosmological Phase Transitions*, *Phys. Rev.* **D 81** (2010) 023004 [arXiv:0905.0643] [INSPIRE].

[93] C. Caprini, R. Durrer and G. Servant, *The stochastic gravitational wave background from turbulence and magnetic fields generated by a first-order phase transition*, *JCAP* **12** (2009) 024 [arXiv:0909.0622] [INSPIRE].

[94] L. Kisslinger and T. Kahniashvili, *Polarized Gravitational Waves from Cosmological Phase Transitions*, *Phys. Rev.* **D 92** (2015) 043006 [arXiv:1505.03680] [INSPIRE].

[95] S.R. Coleman, *The Fate of the False Vacuum. 1. Semiclassical Theory*, *Phys. Rev.* **D 15** (1977) 2929 [*Erratum ibid.* **D 16** (1977) 1248] [INSPIRE].

[96] C.G. Callan Jr. and S.R. Coleman, *The Fate of the False Vacuum. 2. First Quantum Corrections*, *Phys. Rev.* **D 16** (1977) 1762 [INSPIRE].

[97] R. Jinno, T. Konstandin and M. Takimoto, *Relativistic bubble collisions — a closer look*, *JCAP* **09** (2019) 035 [arXiv:1906.02588] [INSPIRE].

[98] D. Bödeker and G.D. Moore, *Can electroweak bubble walls run away?*, *JCAP* **05** (2009) 009 [arXiv:0903.4099] [INSPIRE].

[99] C.J. Moore, R.H. Cole and C.P.L. Berry, *Gravitational-wave sensitivity curves*, *Class. Quant. Grav.* **32** (2015) 015014 [arXiv:1408.0740] [INSPIRE].

JCAP04(2020)001

[100] K. Yagi, N. Tanahashi and T. Tanaka, *Probing the size of extra dimension with gravitational wave astronomy*, *Phys. Rev.* **D 83** (2011) 084036 [arXiv:1101.4997] [INSPIRE].

[101] K. Yagi, *Scientific Potential of DECIGO Pathfinder and Testing GR with Space-Borne Gravitational Wave Interferometers*, *Int. J. Mod. Phys.* **D 22** (2013) 1341013 [arXiv:1302.2388] [INSPIRE].

[102] S. Isoyama, H. Nakano and T. Nakamura, *Multiband Gravitational-Wave Astronomy: Observing binary inspirals with a decihertz detector, B-DECIGO*, *PTEP* **2018** (2018) 073E01 [arXiv:1802.06977] [INSPIRE].

[103] T. Alanne, T. Hugle, M. Platscher and K. Schmitz, *A fresh look at the gravitational-wave signal from cosmological phase transitions*, *JHEP* **03** (2020) 004 [arXiv:1909.11356] [INSPIRE].

[104] USQCD collaboration, *Lattice Gauge Theory for Physics Beyond the Standard Model*, *Eur. Phys. J.* **A 55** (2019) 198 [arXiv:1904.09964] [INSPIRE].

JCAP04(2020)001